Colorado State University Radiation Instrumentation and Data Reduction Procedures for the Convair 990 During Summer Monex

by
Steven A. Ackerman
and
Stephen K. Cox

Department of Atmospheric Science
Colorado State University
Fort Collins, Colorado

Colorado State University

Department of Atmospheric Science

Paper No. 325

COLORADO STATE UNIVERSITY RADIATION INSTRUMENTATION AND DATA REDUCTION PROCEDURES FOR THE CONVAIR 990 DURING SUMMER MONEX

by

Steven A. Ackerman and Stephen K. Cox

Research supported by
The National Science Foundation (under
Grant ATM 78-12631) and a
Grant by the Eppley Laboratory, Inc.

Department of Atmospheric Science
Colorado State University
Fort Collins, Colorado

April, 1980

Atmospheric Science Paper Number 325

ABSTRACT

The basic system design and the radiative instrumentation maintained by Colorado State University on board the Convair 990 jet aircraft during the Summer Monsoon Experiment (MONEX) are described. Calibration procedures are discussed in detail and the derived constants used to convert instrument output to engineering units are given. Specific problems encountered during data reduction and the methods used to overcome them are also discussed. This report should assist meticulous users of the radiation data in obtaining a high quality data set.

ACKNOWLEDGEMENTS

The authors express their appreciation to Mr. Curt Vogel, Ms. Pauline Martin, Ms. Sandy Wunch and Mr. Mark Howes for their role in the preparation of this manuscript. Special thanks are extended to Mr. Randy Horn for his invaluable assistance in instrumentation maintenance during the Summer Monsoon Experiment, and to the personnel aboard the NASA-AMES CV 990 research aircraft. Computer time was provided by the computing facility at NCAR which is sponsored by the National Science Foundation.

This research has been supported by the National Science Foundation under grant number ATM 78-12631.

TABLE OF CONTENTS

LIST OF TABLES

LIST OF FIGURES

LIST OF FIGURES

I. INTRODUCTION

Colorado State University's participation in the 1979 summer Monsoon Experiment (MONEX) field program included the responsibility for collecting cloud microphysics and radiation data on board the NASA-AMES Research Center Convair 990 jet aircraft (CV 990). The primary application of these data is to assist in the development of parameterization schemes to be used in the determination of the large scale radiation convergence profiles of the Indian Summer Monsoon. The Colorado State University instrumentation on board the CV 990 may be classified into four groups:

1) Radiation budget measurements
2) Radiation temperature measurements
3) Angular radiance measurements
4) Cloud microphysics and aerosol measurements.

This report discusses the instrumentation and data reduction procedures used for the radiation budget measurements and radiation temperature measurements. Corresponding information on the angular radiance measurements may be found in Davis et al. (1980). Documentation of the cloud microphysics and aerosol data is still in preparation.

The purpose of this report is to provide potential users of the data with a basic description of the instrumentation as well as the calibration and data reduction procedures. Three types of instruments are discussed.

1) Pyranometers - used to measure solar fluxes (.3 - 2.8 μm and .7 - 2.8 μm)

2) Pyrgeometers - used to measure longwave fluxes (.4 - 50 μm)

3) Bolometer - used to sample temperature fluctuations (Albrecht et al., 1979).

Calibration factors and equations needed to convert raw voltages stored on magnetic tape to engineering units are given. Specific problems resulting from instrument mounting configurations and encountered in the data reduction are discussed.

Appendix A lists the CV-990 flights flown during summer MONEX, along with a brief description of the mission objectives. Also given are depictions of the flight patterns flown to accomplish the objectives of specific radiation missions. A flight-by-flight log of the instrumentation performance is given in Appendix B.

II. BASIC SYSTEM DESIGN

The Colorado State University radiometric instrumentation on board the CV 990 is listed in Table 1. Figure 1 is a schematic of the basic measurement systems. The outputs of all instruments were monitored and recorded on board the aircraft at a station site allocated to Colorado State University. The output voltages were then delivered to the aircraft computer system for recording, monitor display and output of the quick look data set. The thermopile outputs of the pyranometers and pyrgeometers are in the mv range and, therefore, are linearly amplified to a 0-10V scale. To ensure a stable temperature environment, the bottom amplifiers were encased in an insulated container along with a temperature controlled heater.

Three recording systems were used. The primary system was the Airborne Digital Data Acquisition System (ADDAS) supplied by NASA. Angular radiance transducer output voltages were recorded once every second, whereas the pyrgeometer, pyranometer and the Barnes Precision Filter Radiometer (PRT-6) data were scanned and recorded every half second. The back-up system was located at the Colorado State University aircraft station site and consisted of a Monitor Laboratories Model 9100 Data System interfaced with a Cipher Model 70H magnetic tape recorder. This system recorded 29 channels usually at a scan interval of 1 per second. On some missions (Appendix B) the scan rate was increased to 10 per second. The third system was an Easterline Angus paper tape recorder. This system was used primarily as a monitoring device to check instrument operation. The channel assignments for each of the three systems is given in Table 2.

INSTRUMENT	FUNCTION
Pyranometers	Measure the .3 - 3 μm and .7 - 3 μm radiative fluxes
Pyrgeometers	Measure the 4 - 50 μm radiative fluxes
"Bugeye"	Measure the spatial and temporal variations in radiance patterns
PRT-6	Sample air/cloud temperature deviations

Table 1. Colorado State University radiometric instrumentation on board the CV 990.

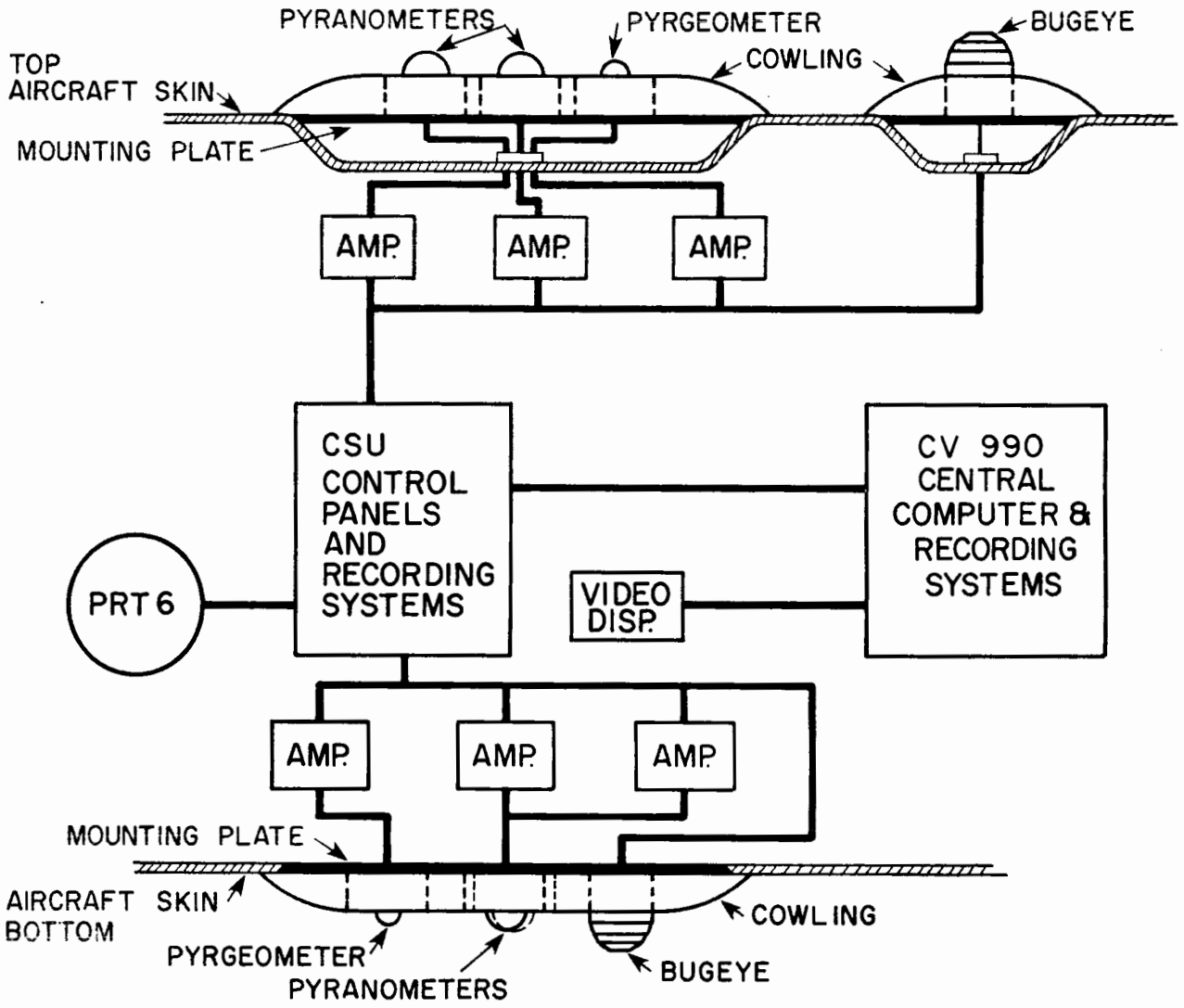

Figure 1. Basic measurement systems and set up.

SIGNAL		ADDAS CHANNEL	MONITOR LABS CHANNEL	EASTERLINE ANGUS CHANNEL
Top RG695 pyranometer		47	0	0
Bottom RG695 pyranometer		48	1	1
Top WG7 pyranometer		49	2	2
Bottom WG7 pyranometer		50	3	3
Top pyrgeometer thermopile output		51	4	4
Top pyrgeometer dome temperature		53	5	5
Top pyrgeometer sink temperature		56	6	6
Bottom pyrgeometer thermopile output		52	7	7
Bottom pyrgeometer dome temperature		54	8	8
Bottom pyrgeometer sink temperature		55	9	9
Top bugeye photodiode number	1	57		10
" " " "	2	58		11
	3	59		12
	4	60		13
	5	61		14
	6	62		15
	7	63		16
	8	64		17
	9	65		18
	10	66		19
	11	67		20
	12	68		21
	13	69		22
Bottom bugeye photodiode number	1	70	16	23
	2	71	17	24
	3	72	18	25
	4	73	19	26
	5	74	20	27
	6	75	21	28
	7	76	22	29
	8	77	23	30
	9	78	24	31
	10	79	25	32
	11	80	26	33
	12	81	27	34
	13	82	28	35
PRT-6 output voltage		83	12	36
PRT-6 heater voltage		84	13	37
PRT-6 shutter temperature		85	14	38
N/A		86		39
+10 voltage supply		87	10	40
-10 voltage supply		88	11	41
True airspeed reference		89		42

Table 2. CV 990 instrument output channel assignments for the three data recording systems.

Two pyranometers, a pyrgeometer and a bugeye instrument were mounted on the top and bottom of the aircraft fuselage. The bottom instruments were located aft of the front wheel well while the top instruments were just forward of the wings. The alignment of these four instruments was different for the top and bottom of the plane as shown in Figure 2. The pyranometers, pyrgeometers and bugeyes were encased in a fiberglass cowling to increase the smoothness of the aerodynamic flow around the instruments. The cowling covered the bases of the radiometers and, therefore, did not affect the field of view of the instruments. The positioning of the cowling is shown in Figure 1. Although the cowling may have improved the aerodynamic flow about the plane, the effect on the pyranometers and pyrgeometers themselves was to decrease their performance. The cowling served as an insulator around the radiometer bases resulting in large dome-sink temperature differences. The resulting errors and correction terms are discussed in Section 4. Dome-sink temperature differences on the bottom radiometers ($\sim$ -6°C at flight altitude) were much larger than for the top instruments ($\sim$ -1°C at flight altitude). These differences are also probably a result of the mounting configurations. The bottom radiometers were on a metal plate which was then mounted on the airplane. The back of this metal plate is part of the floor of an inner compartment inside the plane (Figure 1). Although this compartment was not heated, it was significantly warmer than the outside environment. For the top radiometers, the mounting plate was not in direct contact with the skin of the plane (Figure 1), resulting in a smaller heat transfer from the plane to the radiometer bases reducing differences in the dome and sink temperatures.

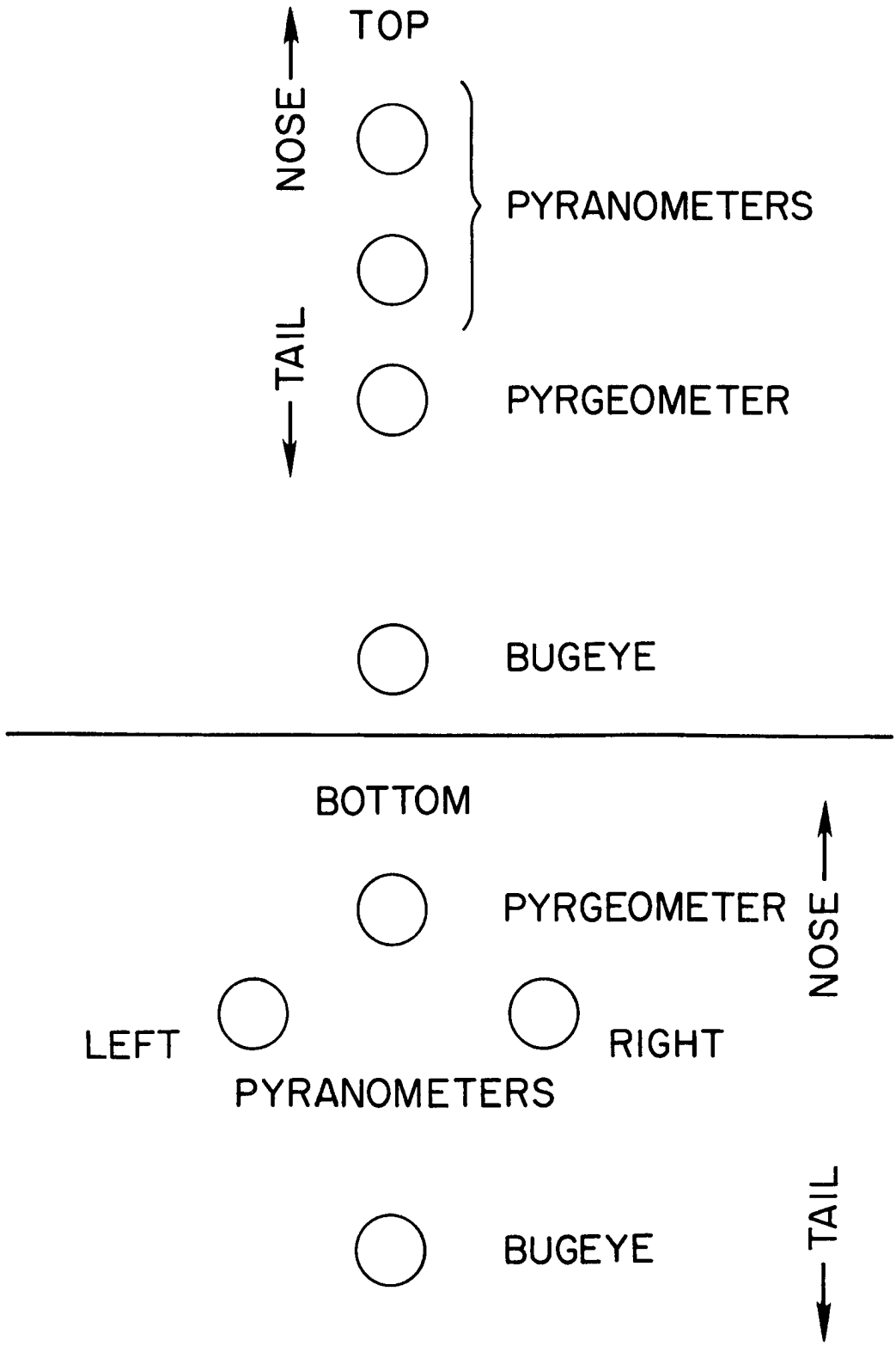

Figure 2. Alignment of radiometers on the CV 990 during MONEX.

The Barnes Precision Filter Radiometer (PRT-6) was mounted horizontally on the portside of the aircraft to the rear of the front passenger loading door. The output voltages were scanned and recorded twice per second. An objective lens with a 2° field of view was used along with a narrow band 15 μm interference filter. A manually operated shutter separated the PRT-6 from the environment. A thermistor was attached to the inside of this shutter to provide in-flight calibration of the PRT-6.

III. AMPLIFIERS

As noted earlier, the outputs of the pyrgeometers and pyranometers were in the mv range and were therefore linearly amplified, using Acromag Model 311 By-u thermocouple amplifiers, to a range of approximately 0-10 volts (V). For the pyranometer amplifiers a 0 mv input corresponds approximately to a .5V output of the Acromag and 25 mv input corresponds to approximately 10.5V output. For the pyrgeometers the amplifiers were set such that -3.0 mv input corresponds to a .5V output and a 1 mv input corresponds to a 10.5V output. The voltages stored on tape may be converted from V to mv using

$$V_o = b_o + b_1 V_a \qquad (1)$$

where V_a = output of the amplifiers in volts

V_o = output of the radiometer in millivolts

$b_o \simeq -1.25$; $b_1 \simeq 2.5$ for the pyranometers*

$b_o \underset{\sim}{\sim} -3.2$; $b_1 \underset{\sim}{\sim} .4$ for the pyrgeometers*.

Errors in determining b_o and b_1 will result in uncertainties in the radiative flux components, however these errors are small. The value of b_o was monitored each flight (Table 3) by electrically shorting the input to the amplifiers. b_1 was determined once in Saudi Arabia and once in India as is given in Table 4. The induced error on the pyranometer output by using the wrong b_1 may be estimated by

---

*See Table 3 for more precise values of these constants.

CV 990 FLIGHT NUMBER	PYRANOMETER POSITION/DOME TYPE				PYRGEOMETER POSITION	
	TOP/RG695	BOTTOM/RG695	TOP/WG7	BOTTOM/WG7	TOP	BOTTOM
3	-1.255	-1.238	-1.258	-1.245	-3.242	-
4	-1.275	-1.225	-1.25	-1.24	-3.243	-
5	-1.240	-1.233	-1.255	-1.24	-3.244	-
6	-1.248	-1.258	-1.27	-1.26	-3.21	-3.211
7	-1.258	-1.265	-1.278	-1.265	-3.226	-3.215
8	-1.26	-1.265	-1.28	-1.268	-3.226	-3.212
9	-1.26	-1.270	-1.275	-1.275	-3.224	-3.228
10	-1.288	-1.273	-1.263	-1.265	-3.216	-3.218
11	-1.264	-1.258	-1.268	-1.266	-3.176	-3.243
12	-1.261	-1.253	-1.27	-1.261	-3.202	-3.251
13	-1.244	-1.255	-1.273	-1.266	-3.205	-3.265
14	-1.254	-1.248	-1.275	-1.258	-3.204	-3.253
15	-1.249	-1.260	-1.283	-1.273	-3.206	-3.269
16	-1.264	-1.25	-1.263	-1.258	-3.189	-3.257
17	-1.261	-1.248	-1.263	-1.266	-3.184	-3.263
18	-1.261	-1.258	-1.27	-1.271	-3.190	-3.25
19	-1.264	-1.255	-1.265	-1.263	-3.177	-3.252
20	-1.279	-1.255	-1.263	-1.263	-3.178	-3.25
21	-1.261	-1.258	-1.265	-1.261	-3.179	-3.252
22	-1.264	-1.255	-1.263	-1.261	-3.176	-3.246
23	-1.266	-1.255	-1.278	-1.266	-3.215	-3.265
24	-1.266	-1.255	-1.278	-1.266	-3.213	-3.264
25	-1.259	-1.25	-1.27	-1.271	-3.214	-3.271
26	-1.261	-1.260	-1.27	-1.271	-3.195	-3.261
27	-1.266	-1.26	-1.278	-1.286	-3.208	-3.269
28	-1.276	-1.26	-1.28	-1.296	-3.213	-3.281
29	-1.279	-1.26	-1.288	-1.288	-3.208	-3.283
30	-1.256	-1.26	-1.28	-1.286	-3.219	-3.283
31	-1.256	-1.270	-1.303	-1.291	-3.204	-3.303

Table 3. Zero offsets (b_o) in volts associated with each Acromag amplifier as a function of CV 990 flight number. Top and bottom refer to location on the aircraft fuselage. Dome type refers to the spectral region measured by the pyranometer; RG695 measures the .7 - 3 μm spectral region while the WG7 measures the .3 - 3 μm regime.

CV 990 FLIGHT NUMBER	PYRANOMETER POSITION/DOME TYPE				PYRGEOMETER POSITION	
	TOP/RG695	BOTTOM/RG695	TOP/WG7	BOTTOM/WG7	TOP	BOTTOM
3 - 10	2.5	2.5	2.5	2.5	.4	.4
11 - 31	2.483	2.476	2.486	2.482	.396	.404

Table 4. Slope (b_1) associated with each Acromag amplifier as a function of CV 990 flight number. Top and bottom refer to instrument locations on the aircraft fuselage. Dome type refers to the spectral region measured by the pyranometer.

assuming there is no error in determining the value of b_o. The resulting error in the pyranometer output can then be written as

$$\frac{V_o' - V_o}{V_o} = \frac{(b_1' - b_1)\ Va}{V_o} \qquad (2)$$

where V_o is determined by assuming $b_o = -1.25$ and $b_1 = 2.5$ and V_o' is calculated assuming $b_o = -1.25$ and a b_1'. Analogous to the method described above, percent errors resulting from an error in b_o can be determined by assuming a known slope, b_1. A similar procedure may be carried out for the pyrgeometers. The estimated error resulting from an error in b_o and/or b_1 is less than 2%.

IV. PYRANOMETER DESCRIPTION AND CALIBRATION PROCEDURES

The pyranometers used on board the CV 990 were Eppley precision spectral pyranometers and have been described by Albrecht and Cox (1976) and Robinson (1966). Fundamentally, the instrument is a thermopile with the incident radiation being the source of the temperature difference between the hot and cold junctions. The spectral region is chosen by use of a hemispheric dome with the appropriate spectral characteristics. For the MONEX Experiment two types of domes were used:

1) WG7 domes were used to measure the .3 - 2.8 μm spectral region
2) RG695 domes were used to measure the .7 - 2.8 μm spectral region.

The transform equation from the millivolt (mv) output of the pyranometer to watts per square meter ($W\ m^{-2}$) is of the form

$$\text{IRRADIANCE} = (\text{Pyranometer output})/k \qquad (3)$$

where k is a function of the cold junction or sink temperature and the individual instrument characteristics. The temperature dependence of k is weak so that a constant value is assumed as given in Table 5. The pyranometer output voltage is approximately 8×10^{-3} mv per $W\ m^{-2}$. Because of this small signal the output voltage was amplified, in a linear fashion, to a range of 0 - 10 V as discussed previously.

Prior to the experiment three of the five pyranometers used in the MONEX Experiment were calibrated at the NOAA/Enviornmental Research

CV 990 FLIGHT NUMBER	PYRANOMETER SERIAL NUMBER	k $mv/(Wm^{-2})*10^{-3}$	M	B	a_0	a_0'	a_1'	POSITION ON AIRCRAFT	TYPE OF DOME
3 - 11	12513	8.57	.99716	1.78032	4.44	-5.4559	.5096	Top	RG695
	12512	7.39	.98997	.696	10.2	-.7131	3.7643	Bottom	RG695
	12515	8.93	1.	-1.37	-1.46	-2.2709	.7734	Top	WG7
	12511	7.95	.99875	4.68154	11.97	-7.0008	1.7015	Bottom	WG7
12 - 26	12514	9.69	.99552	-1.37752	16.82	2.2746	2.3858	Bottom	RG695

Table 5. Constants used to convert pyranometer output voltages (in mv) to irradiance ($W\ m^{-2}$).

Laboratories, Boulder, CO. To intercompare all five instruments the pyranometers were mounted on the roof of the Atmospheric Science Building at Colorado State University. All instruments agreed to within $\pm$ 5 W m^{-2}. A "standard" pyranometer was chosen and each instrument was adjusted for a slightly better comparison. The fitted equation is linear;

$$\text{Corrected irradiance (W m}^{-2}) = M \times \text{measured irradiance (W m}^{-2}) + B. \quad (4)$$

The constants M and B are listed in Table 5.

Further intercomparison tests were possible during the transit flights to and from the MONEX region. During these flights WG7 domes were installed on all the pyranometers allowing intercomparisons of the two top and the two bottom instruments. A large portion of one transit flight was a night flight. This flight was advantageous in determining an optical zero offset for the instruments flown during that flight. Determination of the optical zeros of the pyranometers was the next step in the calibration procedure.

The optical zero offset depends on several processes which affect the temperature difference between the inner dome and the thermopile; these include heat transfer between the mounting plate and the pyranometer base and the heat transfer between the environment and the pyranometer. When these processes are in an approximate state of equilibrium the optical zero offset is constant. This constant optical zero value, a_0, is given in Table 5.

During ascent or descent the pyranometer is not necessarily in equilibrium. Figure 3 presents a plot of the 5 sec average optical zero value of pyranometer #12514 as a function of the dome-sink temperature difference of the bottom pyrgeometer. Each symbol corresponds to a certain hour of the flight and thus the plot can also be viewed as a time series. A similar relationship holds for the other three pyranometers. The actual dome-sink temperature difference of the pyranometer is probably less than the difference measured by the pyrgeometer thermistors since the inner dome of the pyranometer is protected from the outside environment by an outer dome. The initial rate of change of the pyranometer dome-sink temperature difference is also probably less than that of the pyrgeometers. Thus, application of the optical zero correction using the dome-sink temperature difference of the pyrgeometer may result in an over-correction, particularly during the ascent or descent of a flight leg.

Two plausible correction terms for the optical zero offset of the pyranometers are apparent. The first is a constant correction term, a_0, which is representative of the offset provided the dome and sink temperatures of the pyranometers are in approximate thermal equilibrium. The second method is a linear relationship dependent upon the dome-sink temperature difference, i.e.

$$\text{Correction} = a_0' + a_1' (T_D - T_S) \qquad (5)$$

where T_D = dome temperature of the pyrgeometer

T_S = sink temperature of the pyrgeometer.

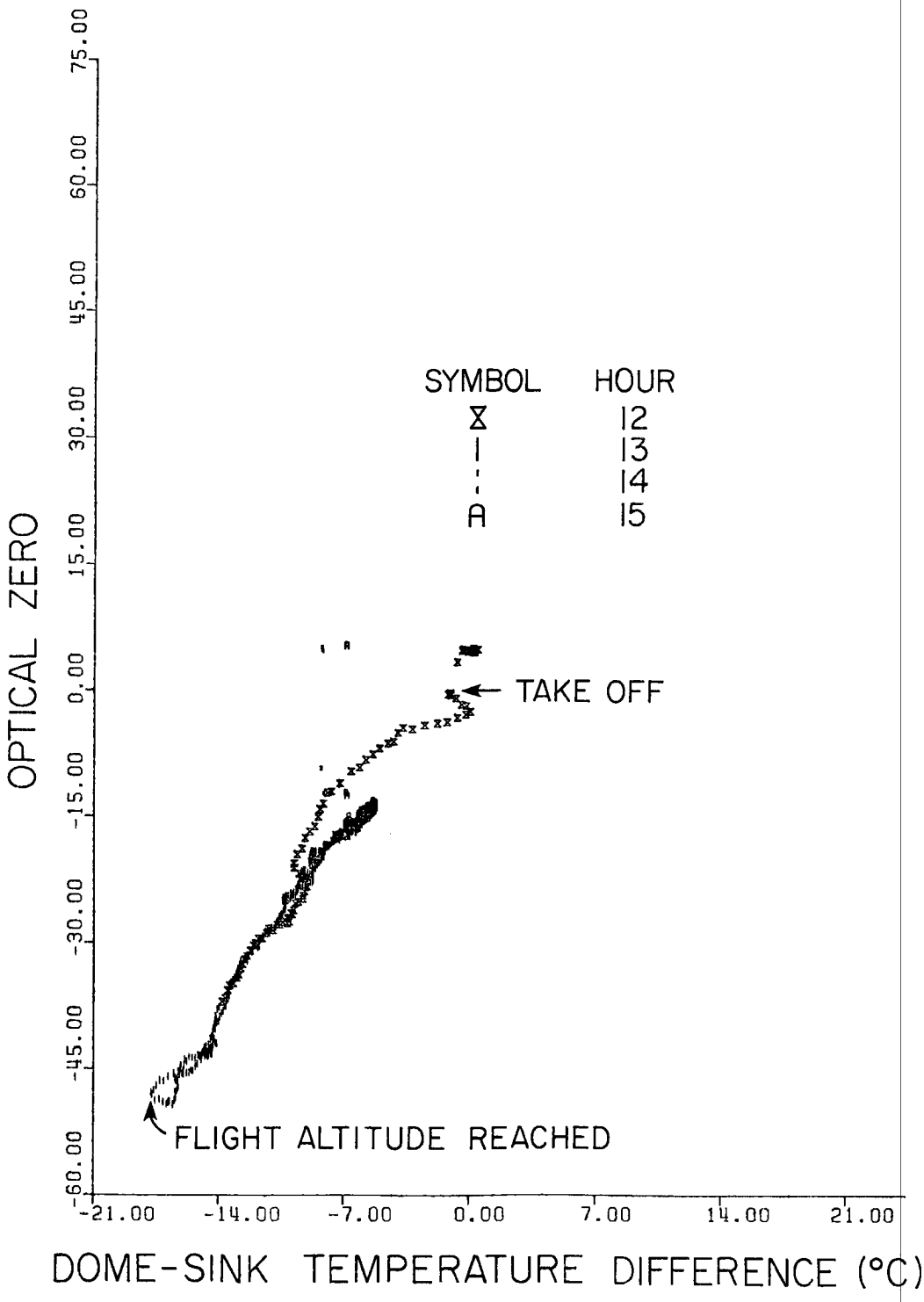

Figure 3. Optical zero ($W\ m^{-2}$) of pyranometer serial number 12514 as a function of the dome-sink temperature difference of the bottom pyrgeometer. Each symbol corresponds to a given hour.

This method is only as accurate as the assumption that the dome and sink temperature difference of the pyranometers is proportional to the dome-sink temperature difference of the pyrgeometers. During rapid ascents or descents application of this method may result in an overcorrection. Overcorrection may also occur at the beginning of a new, constant flight altitude after having ascended or descended from a previous altitude, e.g. during stair-step patterns.

The two methods outlined above were used to derive the optical zero for four of the five pyranometers. Shortly after arriving in India, the bottom pyranometer measuring the .7 - 2.8 μm spectral region was replaced. Since there were no night flights prior to this replacement, a different method was used to determine the optical zero of the initial bottom near IR pyranometer, serial number 12512. The bottom pyranometer measuring the .3 - 2.8 μm spectral region (serial number 12511) was present during the entire experiment, hence its correction function for the optical zero is known. In the transit flights from San Francisco to Dhahran, Saudi Arabia, all pyranometers were mounted with WG7 domes. The difference between the corrected measurement of pyranometer serial number 12511 and the uncorrected measurement of pyranometer serial number 12512 was used to determine the optical zero of pyranometer serial number 12512. The constants a_0, a_0' and a_1' for the five pyranometers are given in Table 5.

To compare the results of applying the two different optical zeros the data collected during flight number 11 was analyzed. Flight number 11 was chosen because of the relatively cloud and dust free state of the atmosphere. A vertical profiling racetrack pattern was flown consisting of six different flight altitudes at approximately

37000, 25500, 17000, 2900, 1050 and 500 feet. A 1/8 - 2/8 cloud cover between approximately 2900 and 1500 feet was observed. The measured fluxes computed using the two techniques for the optical zero correction at the end of each flight altitude for the .3 - 2.8 μm spectral region are shown in Figure 4. Also shown are the calculated fluxes computed from a broadband radiative transfer model described by Cox and Griffith (1979a). In this model a "clear" atmosphere is assumed (e.g. cloud and dust free), a standard tropical atmosphere vertical distribution of O_3 was assumed as well as the standard tropical atmosphere temperature and moisture profiles above the maximum flight altitude ($\sim$ 235 mb). Below the maximum flight altitude flight data temperature and moisture profiles were used. The vertical distribution of carbon dioxide was assumed constant at .486 g/kg. The measured fluxes are not corrected for the pitch or roll of the plane. The calculated fluxes at each altitude are computed using a time representative of the time of day that the flight leg was flown to account for the cosine response of the instrument. Disagreement between the two methods applied to the top WG7 pyranometer (measuring the .3 - 2.8 μm spectral region) are small. Differences between the measured and calculated downward fluxes are larger and may be an artifact of the unknown state of the atmosphere above the maximum flight altitude. The difference between the measured upward fluxes is a maximum, approximately 6 W m^{-2} at the lower flight altitudes where the $T_D - T_S$ is the largest. This discrepancy may be a result of the misrepresentation of the pyranometer dome-sink temperature difference by the dome-sink temperature difference of the pyrgeometers. Differences in the measured and calculated upward fluxes are generally between 15 - 20 W m^{-2}.

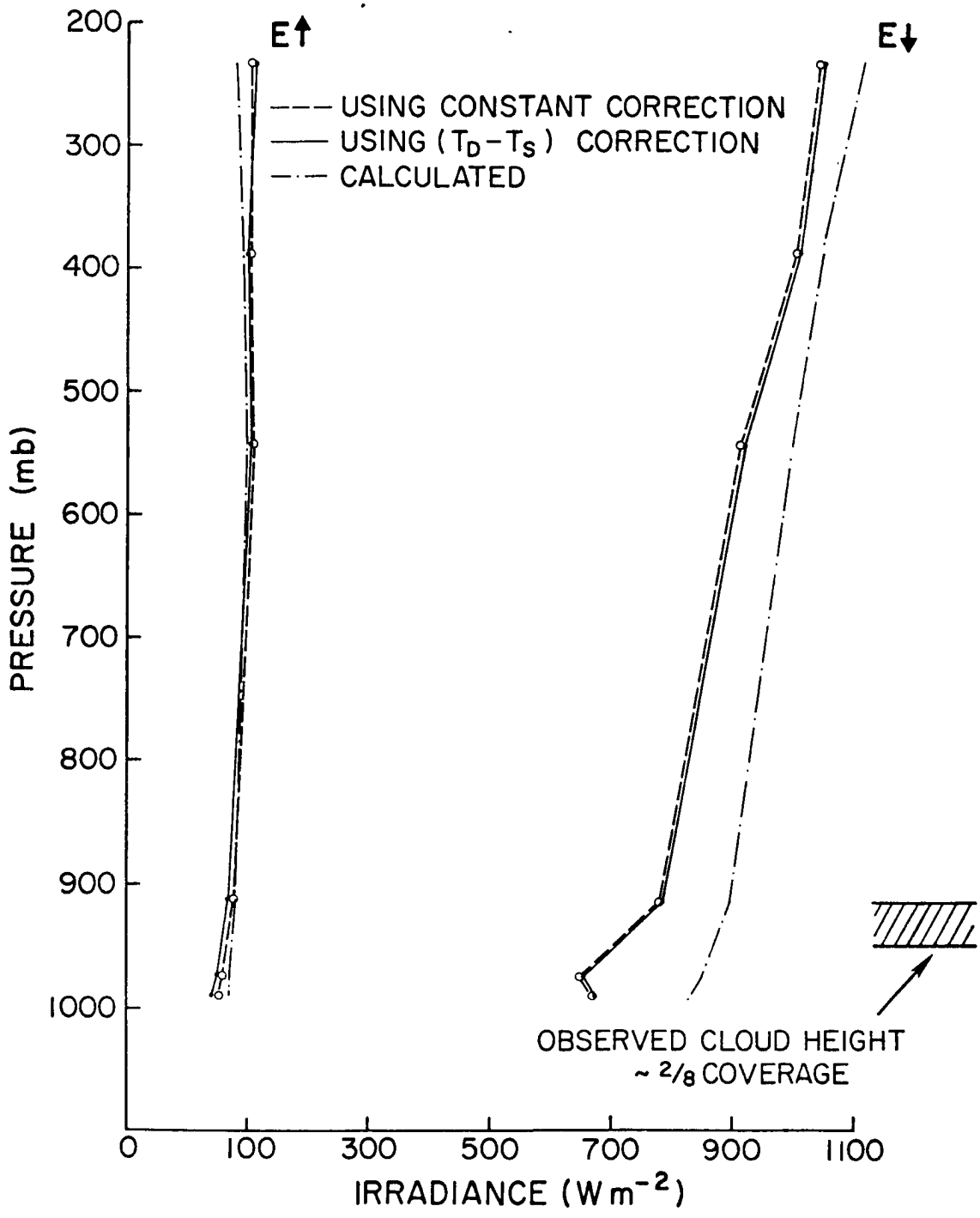

Figure 4. Comparison of the calculated and measured .3 - 2.8 μm radiative fluxes using data from the last two minutes of each of the six flight altitudes of flight number 11.

A similar analysis, Figure 5, for the RG695 pyranometers (measuring the .7 - 2.8 μm spectral region) reveals that the $T_D - T_S$ correction term is approximately 3 W m^{-2} and 10 W m^{-2} less than the result obtained using a constant correction factor for the top and bottom pyranometers respectively.

Calculation of the radiative convergence in the .7 - 2.8 μm spectral region results in an approximate difference of 10 W m^{-2} per flight level interval between the two optical zero correction methods. Differences between the two techniques in computing the radiative convergence in the .3 - 2.8 μm spectral region are approximately 5 W m^{-2} per flight level interval. Except for the 2900-1050 AGL (914 - 973 mb) flight altitudes, the $T_D - T_S$ correction term results in a smaller radiative convergence for both the .3 - 2.8 and .7 - 2.8 μm spectral regimes.

Figure 6 is a time series plot of the measured irradiances of the bottom RG695 pyranometer derived using the two optical zero correction terms. From this figure it is evident that the $T_D - T_S$ correction is largest after having descended to a new flight altitude. Differences between the two techniques range from approximately 10 W m^{-2} to -12 W m^{-2}. Application of the $T_D - T_S$ correction term can produce negative irradiances emphasizing the problems with using the dome and sink temperatures of the pyrgeometers. The dome of the pyrgeometer is directly exposed to the air flow about the plane and hence responds rapidly to temperature changes in the air. In the case of the pyranometers, the dome temperature that is sensed by the thermopile is protected from direct air flow by an outer dome and therefore,

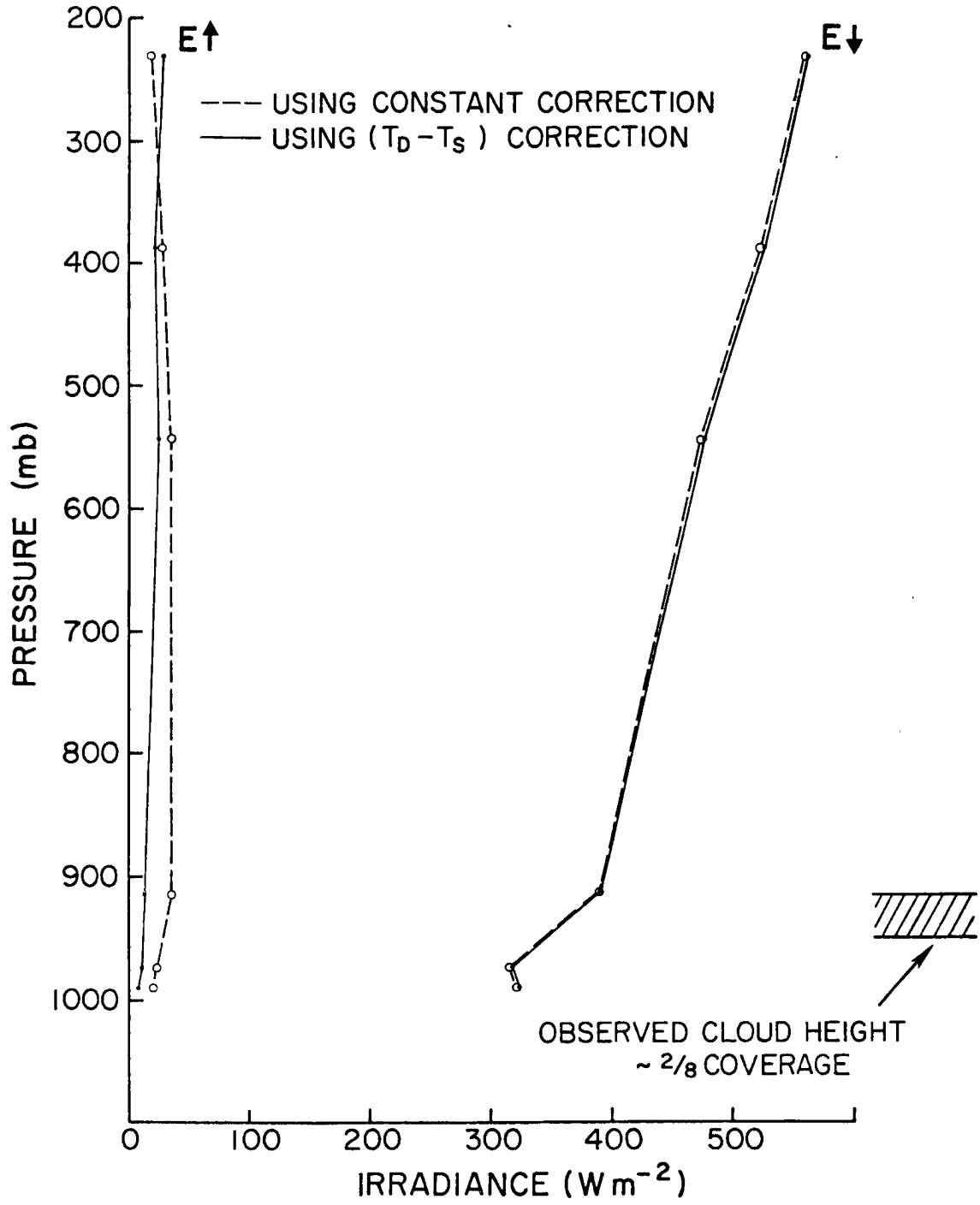

Figure 5. Intercomparison of the measured .7 - 2.8 μm radiative fluxes using data from the last two minutes of each of the six flight altitudes of flight number 11.

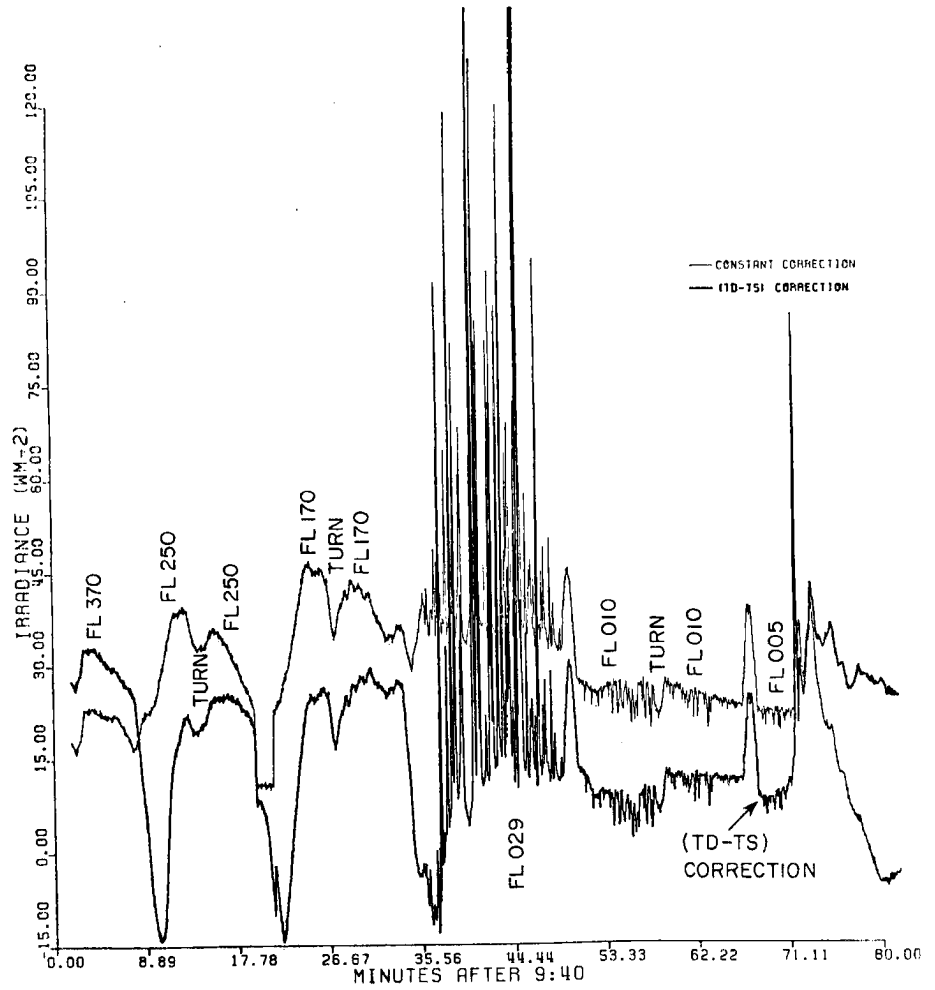

Figure 6. The measured upward flux in the .7 - 2.8 μm spectral region using the two optical zero correction methods.

temperature fluctuations will not be as large as those of the pyrgeometer dome.

The RG695 and WG7 pyranometers will also be used to determine the radiative fluxes in the visible region of the solar spectrum (.3 - .7 μm) as well as the albedos of various surfaces. In the case of the visible spectral fluxes differences between the $T_D - T_S$ and the constant correction functions for the downward and upward fluxes are approximately +3 W m^{-2} and +6 W m^{-2} respectively. These differences are generally uniform throughout the racetrack pattern and will therefore cancel in the radiative convergence calculations. Figure 7 is a time series plot of the downward flux in the .3 - .7 μm spectral region determined from application of the two optical zero corrections. Although there tends to be an offset between the two derived values the time rate of change of the two are essentially identical.

The .3 - 2.8 μm albedos calculated using the $T_D - T_S$ optical zero correction are consistently less than the constant correction method by approximately .005 to .01. The difference between the $T_D - T_S$ and the constant correction function in determining the albedo in the .7 - 2.8 μm region is approximately .01 to .03.

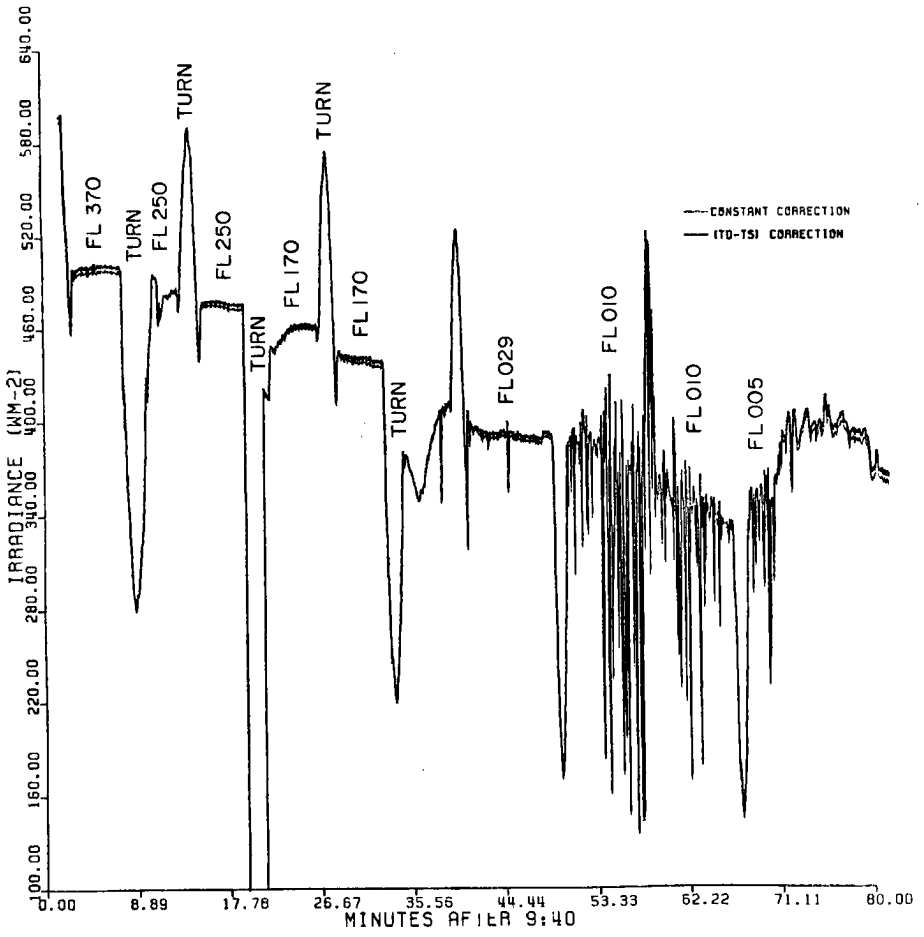

Figure 7. Time series plot of the downward radiative flux in the .3 - .7 μm spectral region derived from the two optical zero correction functions applied to the RG695 and WG7 pyranometers.

V. PYRGEOMETER DESCRIPTION AND CALIBRATION PROCEDURES

The pyrgeometers used to measure the longwave fluxes ($\sim$ 4 - 50 μm) were similar to those described by Albrecht et al. (1974). The pyrgeometers consist of a thermopile beneath a KRS-5 or a silicon hemispheric dome. The type of dome used as a function of flight is given in Table 6. The inside of the domes are coated with an interference filter which prevents the transmission of the shorter wavelengths (< 3.5 μm). Albrecht and Cox (1976) suggest that the pyrgeometer dome and sink temperatures be monitored for a more accurate determination of the incident fluxes. Bead thermistors were used to monitor the dome and the thermopile cold junction or sink temperature. The longwave radiation incident on the pyrgeometer is given by

$$E = K_1 V_0 + \sigma\varepsilon_0 T_S^4 - K_2 \sigma(T_D^4 - T_S^4) \qquad (7)$$

where E = incident longwave radiation

V_0 = output of the pyrgeometer thermopile in mv

σ = Stephan-Boltzman constant

ε_0 = emittance of the thermopile (ε_0 assumed to be 1)

T_D = temperature of pyrgeometer dome (°K)

T_S = temperature of the thermopile cold junction or sink (°K)

K_1, K_2 = constants.

The calibration procedures for obtaining K_1 and K_2 has been described by Albrecht et al. (1974) and Albrecht and Cox (1976). The procedure used is to heat the pyrgeometer dome and then face the

CV 990 FLIGHT NUMBER	PYRGEOMETER SERIAL NUMBER	LABORATORY DERIVED VALUES ($W\ m^{-2}$ per mv)		FIELD DERIVED VALUES ($W\ m^{-2}$ per mv)		POSITION ON AIRCRAFT	TYPE OF DOME
		K_1	K_2	K_1	K_2		
1 - 11	12508	255.22	1.91	257.94	3.21	Top	Silicon
	12507	242.29	2.48	221.69	2.72	Bottom	Silicon
12 - 16	12504	208.88	4.07	220.26	3.66	Top	KRS-5
	12503	252.02	3.62	231.83	4.41	Bottom	KRS-5
17 - 24	12503	230.38	2.41	275.20	4.29	Bottom	Silicon
25 - 31	12504	402.38	4.13	-	-	Top	KRS-5

Table 6. Constants used to convert pyrgeometer output voltages to irradiance values ($W\ m^{-2}$).

pyrgeometer into a black body cavity of known temperature while monitoring the thermopile output voltage and the dome and sink temperatures. As the dome cools, a point is reached when the dome and sink temperature are equal and the instrument sensitivity, K_1, can be determined. The value of K_2 is determined once the instrument sensitivity is known. Figures 8 and 9 are examples of the laboratory calibration results. Figure 8 is a plot of the pyrgeometer thermopile output voltage vs. $\sigma(T_{BB}^4 - T_S^4)$. The slope of the fitted line yields the value of K_1. Figure 9 shows the least squares fitted line that represents the value of K_2. Each symbol represents a calibration run. The small deviations about the fitted line suggest an accurate determination of both K_1 and K_2. However, the field experiment conditions are difficult to reproduce in a laboratory. For example, large dome-sink temperature differences, a rapidly changing dome and sink temperature and dynamic heating of the dome were not adequately simulated in the laboratory calibration. Also, the dome and sink temperatures are measured by a bead thermistor and may not be representative of a mean temperature. During the laboratory calibration, the thermistors are probably representative of the dome and sink temperature since temperature changes are rather slow and uniform. However, on the aircraft there exists dynamic heating of the dome and as a result a single point measurement may not represent the mean dome temperature.

An in-flight calibration of K_1 and K_2 can be accomplished by assuming that the irradiance field emanating from a uniform target (i.e. clear sky, ocean surface, uniform cloud deck) is known. During the CV 990 flight number 11, a stair-step racetrack pattern was flown northwest of Bombay, India. The pattern consisted of six flight

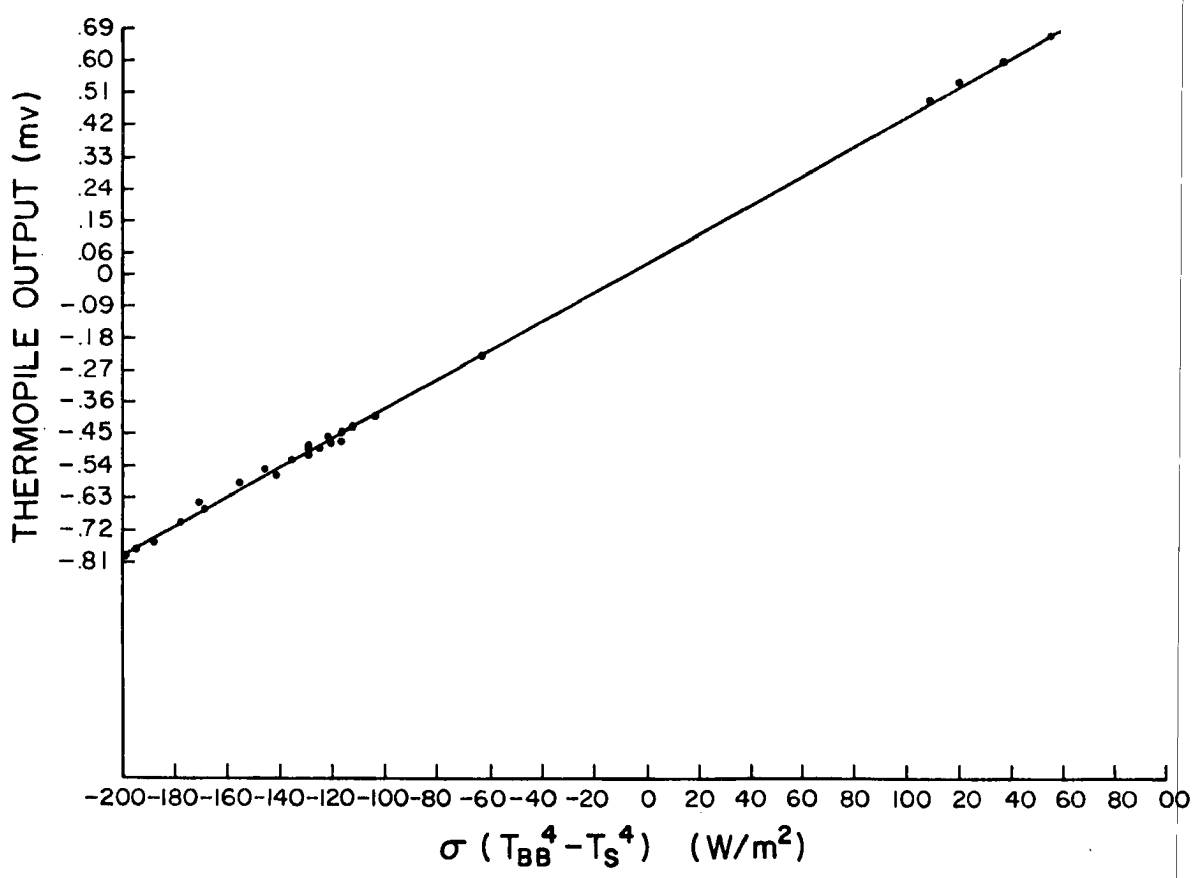

Figure 8. Thermopile output as a function of the radiative energy difference per unit area of the black body and the thermopile sink. The slope of the least squares fitted line is K_1.

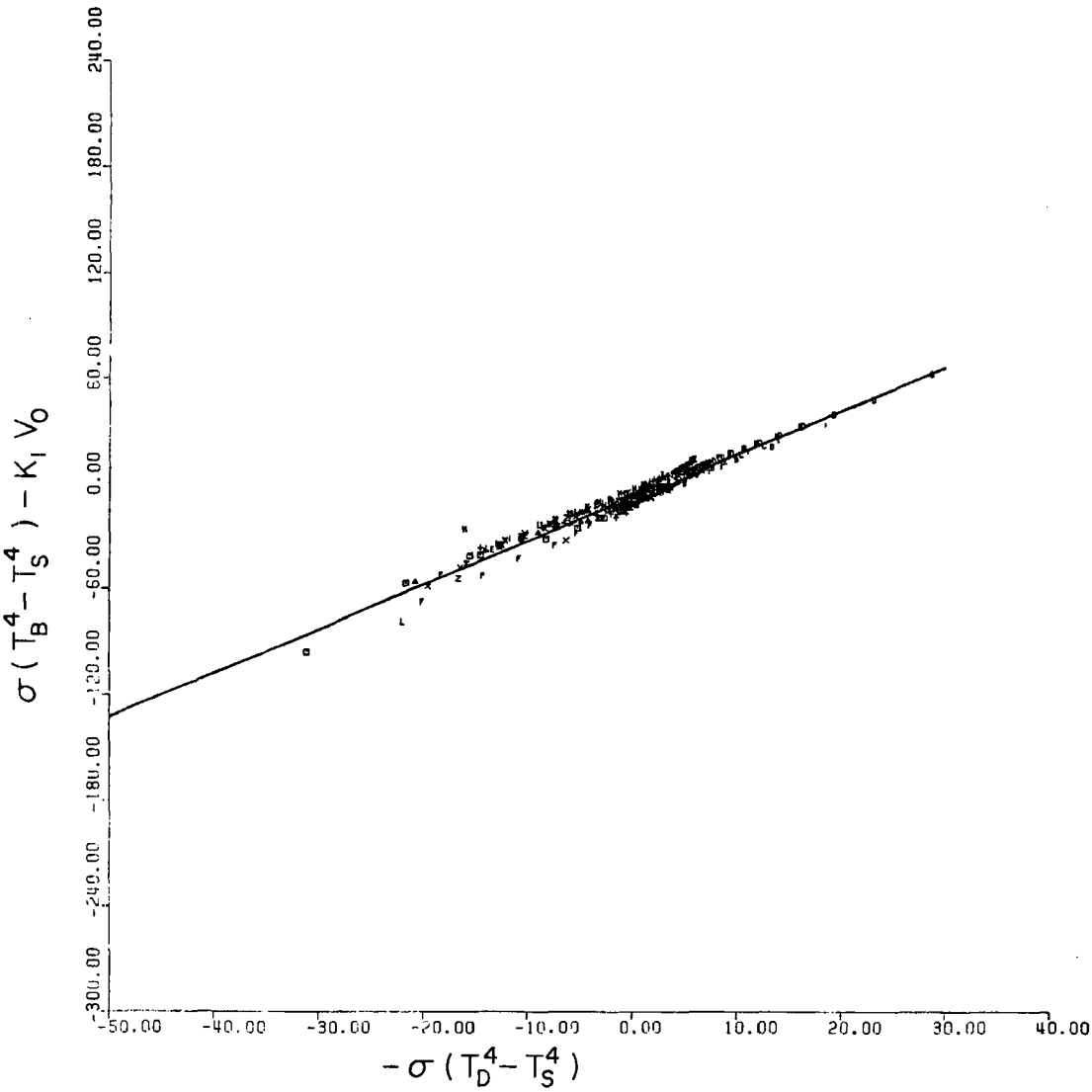

Figure 9. The radiative energy difference per unit area between the black body, thermopile sink and the incident energy on the thermopile versus the radiative energy difference per unit area between the dome and sink of the pyrgeometer. The slope of the fitted line is the value of K_2. Each symbol represents a calibration run.

altitudes averaging in height from 37000 to 500 feet AGL. The weather conditions on this day were scattered stratocumulus with 1/8 - 2/8 coverage. The upward and downward fluxes on this day should have been fairly homogeneous at a given flight altitude. However, application of the laboratory derived values of K_1 and K_2 showed a tendency for both the upward and downward fluxes to decrease during each leg in the racetrack pattern. The irradiance values approached a constant towards the end of each run. This is depicted in Figure 10. Albrecht and Cox (1976) discuss the possible dependence of K_2 on temperature. Assuming an irradiance value and using the laboratory derived value of K_1, a value of K_2 was calculated for each leg of the racetrack pattern. The value of K_2 determined in this manner was consistent with each flight leg suggesting that K_2 is independent of temperature. The tendency of the upward and downward irradiances to decrease over an apparently uniform target, suggests that the laboratory values of K_1 and K_2 were not appropriate during the actual field experiment, for the reasons outlined above.

Flight number 11 was, therefore, used to determine the values of K_1 and K_2 by assuming a uniform target irradiance and using the measured values of T_S, V_0 and T_D in Eq. 7. These field derived values of K_1 and K_2 significantly improved the irradiances observed during flight number 11 (Fig. 10) and other flights where the laboratory values of K_1 and K_2 would have given questionable trends in the irradiance patterns. The values of K_1 and K_2, both from laboratory and in-field calibrations, are given in Table 6.

After flight number 11 both pyrgeometers were replaced. The new pyrgeometers were mounted with KRS-5 domes. To investigate the

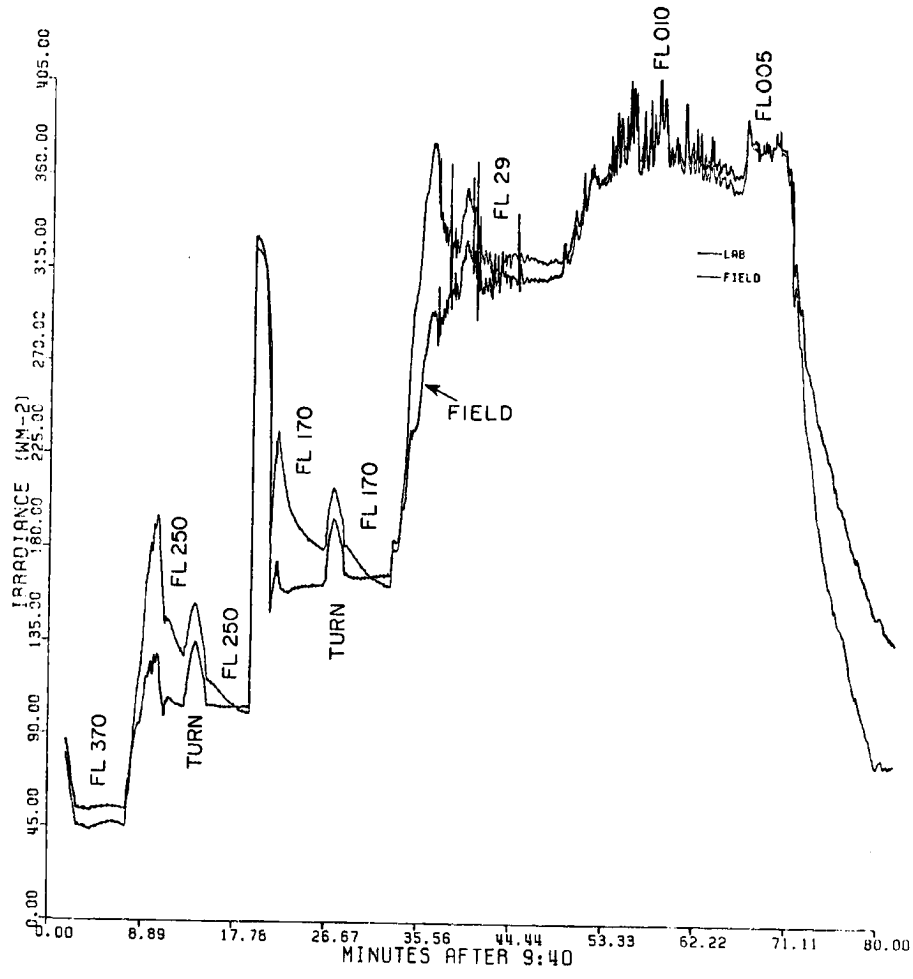

Figure 10. The measured downward irradiance (W m^{-2}) as determined using the laboratory derived constants (LAB) and the field experiment derived constants (FIELD).

accuracy of the laboratory determined values of K_1 and K_2 for these pyrgeometers, flight number 13 was used. During this flight pattern a stair-step descent profile was performed at eight flight levels ranging in height from 35,000 to 500 feet AGL. The pattern was flown over the Arabian Sea where the cloud conditions were 1/8 coverage of trade wind cumulus with cloud tops ranging from 2,500 to 3,000 feet AGL. As with the pyrgeometers flown prior to this flight, questionable trends were observed in irradiance fields when the laboratory values of K_1 and K_2 were used in Eq. 7. As a result, new constants were derived using the flight data from flight number 13 and are given in Table 6.

During CV 990 flight number 16 (Day 158) the bottom pyrgeometer (serial number 12503) KRS-5 dome fell off. The dome was replaced with a silicon dome. Flight number 23 was used for the field calibration of K_1 and K_2 which are applicable to pyrgeometer number 12503 after flight number 16.

During the pre-flight inspection of flight number 25 some corrosion of the top pyrgeometer (serial number 12504) KRS-5 dome was observed. The corrosion was not observed on the section of the dome facing the tail of the aircraft. This corrosion is a result of "sand blasting" during portions of flights that were flown in cloud, dust, etc. in combination with the heavy precipitation of the region.

The KRS-5 dome is a crystal composed of thallium bromide and thallium iodide (44% TlBr and 56% TlI) which is soluable in water. Kozyrev (1966) reported that the transmittance of the KRS-5 dome decreased when the dome was immersed in water. The decrease in the transmittance is spectrally dependent, primarily affecting wavelengths less than 20 μm. Increasing the amount of time the filter is immersed

in liquid water or increasing the water temperature results in a larger decrease of the KRS-5 transmittance. When the dome is polished and clean the effect of liquid water on transmittance is minimized. During each flight some scratching and pitting of the dome occurs allowing water to more readily react with the KRS-5. Prior to flight number 25 there were three days of heavy monsoonal rains which provided sufficient water contact with the KRS-5 dome to reduce its transmittance. Post experiment laboratory derived values of K_1 and K_2 for flight 25-31 are given in Table 6.

The thermistors used to measure the pyrgeometer dome and sink temperature were Yellow Springs Instruments precision bead thermistors type 44006. The following equation can be used to convert thermistor output voltages to temperature:

$$T(°K) = \beta \{\ell n [80 \times V0 (V_0 - V0)^{-1} / K]\}^{-1} \quad (8)$$

where T is the thermistor temperature in °K

V_0 is the positive reference voltage; approximately 10 volts

V0 is the voltage across the thermistor

β and K are constants as given below

for V0 > 6.3	β = 3209.61	K =	$2.503063*10^{-4}$
$6.3 \geq V0 > 3.7$	β = 3344.06	K =	$1.4399*10^{-4}$
$3.7 \geq V0 > 1.9$	β = 3458.48	K =	$9.322*10^{-5}$
$V0 \leq 1.9$	β = 3562.14	K =	$6.4643*10^{-5}$

To compare the results of the two methods used to determine K_1 and K_2, the last two minutes of each of the six flight altitudes of flight number 11 were used to derive the upward and downward fluxes. The results are shown in Figure 11. Also shown in Figure 11 are the calculated fluxes using the infrared radiative transfer routine described in Cox and Griffith (1979a). Temperature, moisture, ozone and carbon dioxide vertical profiles used in the model are described in Section IV.

The agreement between the two calibration techniques is well within the limits of the instrument itself. The agreement between the measured and calculated fluxes is also very good, on the order of 10 - 15 W m^{-2}. The maximum difference between the calculated and measured profiles is approximately 30 - 35 W m^{-2}.

The excellent agreement between the two measured flux profiles is somewhat misleading since they are derived from the last two minutes of data collected at each flight level. The largest differences occur at the beginning of each flight level. Figure 10 is a plot of the downward irradiances measured during the racetrack pattern assuming the laboratory and field derived values of K_1 and K_2. Differences at the beginning of a flight may be as large as 40 - 45 W m^{-2}. During flight number 11 the bottom pyrgeometer was viewing a relatively uniform surface with regard to infrared emittance. Application of the laboratory derived K_1 and K_2 results in questionable trends in the irradiance patterns (Fig. 10). These trends are significantly reduced when the field derived values of K_1 and K_2 are used.

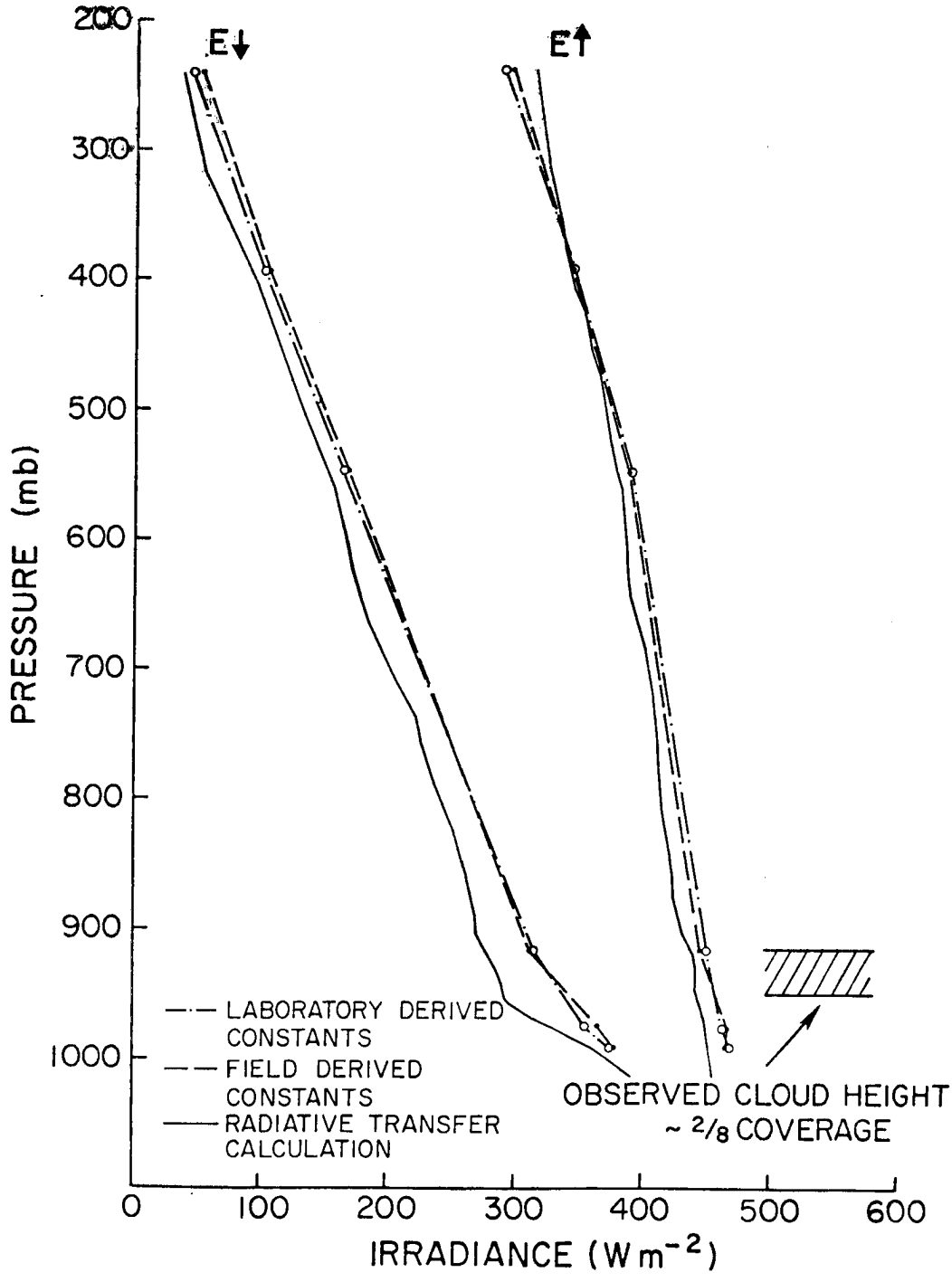

Figure 11. Comparison of the calculated and measured fluxes using data from the last two minutes of each of the six flight altitudes of flight number 11.

VI. BARNES PRECISION FILTER RADIOMETER

The output of the Barnes Precision Filter Radiometer (PRT-6) is a d-c voltage, the magnitude of which is proportional to the energy difference between a target and a known reference. Assuming the field of view of the radiometer is consistently viewing a black body target, the output of the PRT-6 may be written as

$$V = A' \int_{\lambda_1}^{\lambda_2} T(\lambda) \, (B[\lambda, T_{CAVITY}] - B[\lambda, T_{TARGET}]) \, d\lambda \qquad (9)$$

where A' ≡ constant

T ≡ transmittance function dependent on the radiometer optics

B ≡ Planck's Function

λ ≡ Wavelength

T_{CAVITY} ≡ reference temperature of the PRT-6 cavity

T_{TARGET} ≡ temperature of the target occupying the field of view.

To spectrally isolate the incoming energy, a narrow band 15 μm interference filter was placed in front of the detector. Assuming a mean transmittance for the filter spectral region (14.3 - 15.9 μm) and evaluating the Planck function at λ_0 = 15 μm the output of the PRT-6 may be written as

$$V = A \, [B \, (\lambda_0, T_{CAVITY}) - B(\lambda_0, T_{TARGET})]. \qquad (10)$$

Since the temperature of the cavity is maintained at 45°C $\pm$ .25°C, Eq. (10) can be approximated as

$$V = A_0 + A_1 B(\lambda_0, T_{TARGET}). \quad (11)$$

The constants A_0 and A_1 are determined by fitting the PRT-6 output voltage versus the static air temperature during the descent portion of various flight missions. Thus, the temperature of the target occupying the field of view of the PRT-6 can be written as

$$T_{TARGET}\ (°K) = 960 \times \left[\ln\left(A_1 \times 4.925102881 \times 10^8 / (V - A_0)\right) + 1\right]^{-1}$$

where $A_0 = 2.36795$

$A_1 = 3.12595 \times 10^{-7}$.

Figure 12 is a plot of the 1 second mean PRT-6 determined temperature versus the static air temperature during the descent into Bombay at the end of CV 990 flight number 24. Also shown is the line plot which corresponds to equality between the PRT-6 determined temperature and the static air temperature. Major discrepancies between the PRT-6 and static air temperature occur in cloud or after descending through a cloud base. These areas are depicted in the figure and are most probably caused by inadequacies in the static air temperature probe.

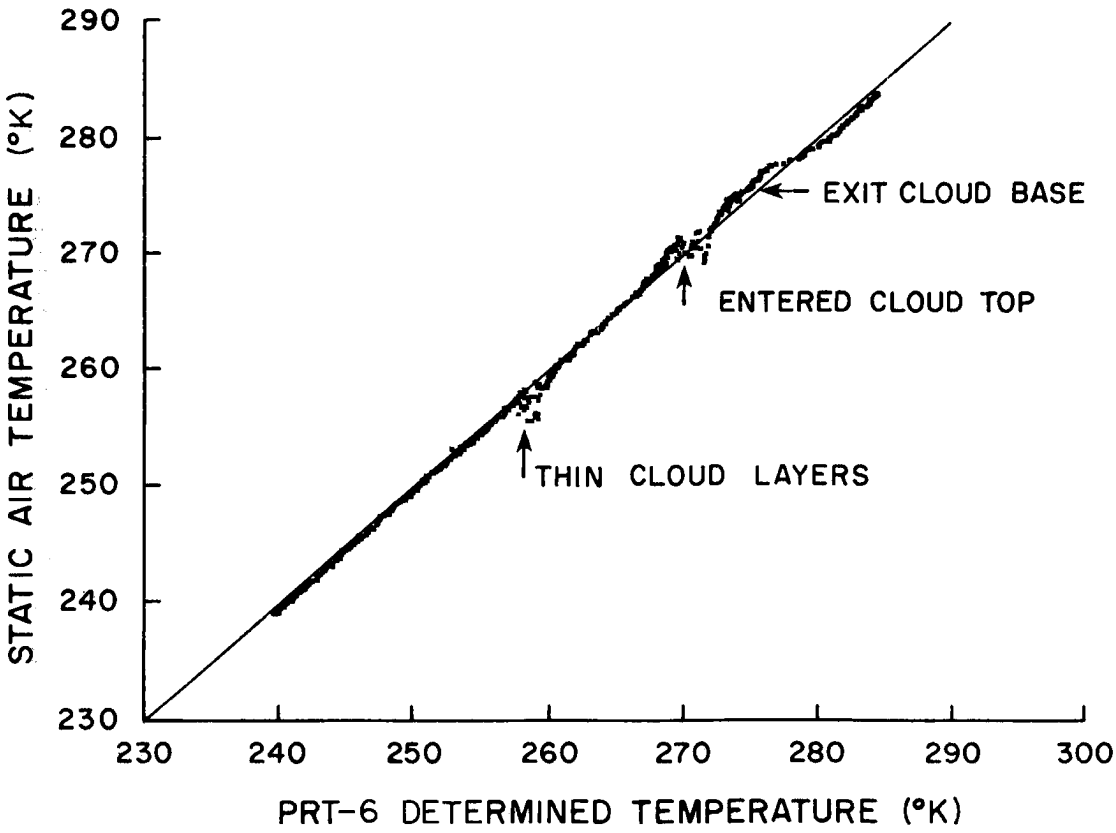

Figure 12. PRT-6 determined temperature versus static air temperature.

VII. SUMMARY

During the summer MONEX field experiment the Convair 990 flew 21 data missions in and around the Arabian Sea region. This report discusses the techniques used to calibrate the pyranometers, pyrgeometers and PRT-6 maintained by Colorado State University. Constant factors and equations needed to convert the raw voltages stored on magnetic tape to engineering units are given. Specific problems that arose during the data reduction are discussed. To date, the data for each of the 21 flights have not been analyzed thoroughly, further problems and questionable data will probably surface as they are more carefully analyzed. However, we believe that the data in their present state are of sufficient quality to render accurate radiative measurements for various scientific application. To assist the user in assessing questionable data, Table 7 lists approximate upper and lower limits of the longwave and shortwave radiative fluxes. The format of the reduced data tape is given in Appendix C.

SPECTRAL FLUX	LOWER LIMIT	UPPER LIMIT
Upward longwave (LW ↑)	$\sigma(T_{AIR})^4$	$\sigma(T_{SURFACE})^4$
Downward longwave (LW ↓)	8	$\sigma(T_{AIR})^4$
Downward shortwave (.3 - 2.8 μm) (SW ↓)	10	1325 X cos(zenith angle)
Upward shortwave (.3 - 2.8 μm) (SW ↑)	.02 X SW↓	SW↓
Downward near IR (.7 - 2.8 μm) (NIR ↓)	.3 X SW↓	.6 X SW↓
Upward near IR (.7 - 2.8 μm) (NIR ↑)	0	.6 X SW↑

Table 7. Upper and lower limits of the energy per unit area ($W\ m^{-2}$) measured by the pyrgeometers and pyranometers.

REFERENCES

Albrecht, B., M. Poellot, and S. K. Cox, 1974: Pyrgeometer measurements from aircraft. Rev. Sci. Instrum., 45, 33-38.

_____, and S. K. Cox, 1976: Radiation data reduction procedures for Sabreliner, C-130 and DC-6 aircraft during the GARP Atlantic Tropical Experiment. Colorado State University Atmospheric Science Paper No. 244, Fort Collins, CO., 100 pp. (NTIS #PB 257 375).

_____, S. K. Cox and W. H. Schubert, 1979: Radiometric measurements of in-cloud temperature fluctuations. Jour. Appl. Meteor., 8, 1066-1071.

Cox, S. K., and K. T. Griffith, 1979a: Estimates of radiative divergence during Phase III of the GARP Atlantic Tropical Experiment, Part I. Methodology. Jour. Atmos. Sci., 36, 576-585.

Davis, J. M., C. Vogel, and S. K. Cox, 1980: A multidirectional photodiode array for the measurement of solar radiances. Submitted for publication in the Rev. Sci. Instrum.

Kozyrev, B. P., 1966: A compensated thermoelectric net radiometer with whitened and bright detecting surfaces protected from air currents by KRS-5 hemispheres. Actinometry and Atmospheric Optics - edited by V. K. Pyldmaa. pp. 168-176.

Robinson, N., 1966: Solar Radiation. Elsevier Publishing Co., Amsterdam, London and New York.

APPENDIX A

CONVAIR 990 FLIGHT SUMMARY DURING SUMMER MONEX

Table A1 is a flight summary of the Convair 990 during summer MONEX. The flight patterns flown during specific radiation missions are depicted in Figures A1 - A5.

SUMMER MONEX CV 990 FLIGHT SUMMARY

DATE	FLIGHT NUMBER	BASE	MISSION TYPE/ LOCATION	OBJECTIVES AND COMMENTS
	1	San Francisco	Test Flight	
	2	San Francisco	Test Flight	
April 30	3A	Moffett, San Francisco	Ferry	Intercomparison of top and bottom pyranometers
April 30	3B	Malmstron, Missouri	Ferry	" " " " " "
May 1	4	Sonderstrom, Greenland	Ferry	" " " " " "
May 3	5	Geneva, Switzerland	Ferry	" " " " " "
May 6	6	Dhahran, Saudi Arabia	Dropwindsonde; land-sea difference	Investigate the land-sea differential heating between Saudi Arabian Desert and Arabian Sea stair-step descent into Dhahran for vertical profiling.
May 9	7	Dhahran	Budget box over the empty quarter region of the Rubal Khali Desert	Define the regional energy budget. Stair step vertical profiling done during "box" pattern.
May 10	8	Dhahran	Budget box over the empty quarter	Investigate regional energy budget flight track essentially the same as flight number 7.
May 12	9	Dhahran	Budget box over the empty quarter	Flight track the same as flight number 7 and 8. This mission was flown in the early morning when the heat low was not as well defined as in flights 7 and 8.

Table A1.

DATE	FLIGHT NUMBER	BASE	MISSION TYPE/ LOCATION	OBJECTIVES AND COMMENTS
May 14	10	Dhahran	Dropwindsonde; land-sea differential heating	Land-sea differential heating study of Saudi peninsula and Arabian Sea. Stair-step vertical profiling done on return leg to Dhahran.
May 18	11	Dhahran	Ferry with vertically stacked racetrack pattern	Racetrack pattern flown over the Arabian Sea west of Bombay, India. Objective was to define the vertical profiles of radiative fluxes, aerosols, cloud microphysics, temperature and moisture.
May 29	12	Bombay, India	Dropwindonde (DWS) survey mission over central Arabian Sea	Investigate heat sources/sinks over central Arabian Sea in pre-monsoonal conditions.
May 31	13	Bombay, India	Budget box pattern over North central Arabian Sea	Study the regional energy budget. A stair-step descent leg was flown on one of the diagonals of the box pattern for vertical profiling.
June 3	14	Bombay, India	DWS survey mission of central Arabian Sea	Investigate heat sources over central Arabian Sea in pre-monsoonal conditions.
June 5	15	Bombay, India	Albedo survey over north central India	Study the radiative characteristics of various terrains. Stair-step descent flight leg was flown between New Delhi and Calcutta.
June 7	16	Bombay, India	DWS Arabian Sea survey mission	Investigate dynamic and thermodynamic fields over the Arabian Sea in pre-monsoonal conditions.

SUMMER MONEX CV 990 FLIGHT SUMMARY

Table A1. (Continued)

DATE	FLIGHT NUMBER	BASE	MISSION TYPE/ LOCATION	OBJECTIVES AND COMMENTS
June 11	17	Bombay	First part of a combined DWS and radiation mission -- albedo survey	Study the radiative characteristics of various terrain. Stair-step vertical profiling was part of the flight. This is the first part of a two flight sequence to investigate meridional differential heating.
June 12	18	Bombay	Second part of a combined DWS - radiation mission - survey	Second part of a two flight sequence to investigate meridional differential heating.
June 14	19	Bombay	Radiation mission -- rosette pattern	Sample the angular distribution of the radiance pattern of the specified cloud field
June 15	20	Bombay	DWS survey mission of Arabian Sea	Investigate the dynamic and thermodynamic fields over the Arabian Sea during the onset of monsoon.
June 17	21	Bombay	DWS survey mission of Arabian Sea	Investigate the dynamic and thermodynamic fields over the Arabian Sea during the onset of monsoon.
June 18	22	Bombay	DWS survey mission of Arabian Sea	Investigate the dynamic and thermodynamic fields over the Arabian Sea during the onset of the SW monsoon.
June 22	23	Bombay	Radiation mission -- racetrack pattern stacked vertically	Sample the vertical distribution of radiative fluxes, aerosols and cloud microphysics.
June 23	24	Bombay	Radiation mission -- rosette pattern	Sample the angular distribution of the radiance pattern of the specified cloud field.

SUMMER MONEX CV 990 FLIGHT SUMMARY

Table A1. (Continued)

DATE	FLIGHT NUMBER	BASE	MISSION TYPE/ LOCATION	OBJECTIVES AND COMMENTS
June 26	25	Bombay	Radiation mission -- stacked racetrack pattern	Sample the vertical distribution of the radiative fluxes, aerosols and cloud microphysics.
June 27	26	Bombay	DWS survey mission of the Arabian Sea	Investigate the dynamic and thermodynamic fields over the Arabian Sea during the SW monsoon.
July 2	27	Bombay	Ferry	ADDAS system inoperative - no A/C data recorded.
July 3	28	Bangkok, Thailand	Ferry	Intercomparison of top and bottom pyranometers.
July 4	29	Hong Kong	Ferry	" " " " " "
July 6	30	Narrita, Tokyo	Ferry	" " " " " "
July 7	31	Anchorage, Alaska	Ferry	" " " " " "

SUMMER MONEX CV 990 FLIGHT SUMMARY

Table A1. NASA Convair 990 Summer MONEX Flight Summary.

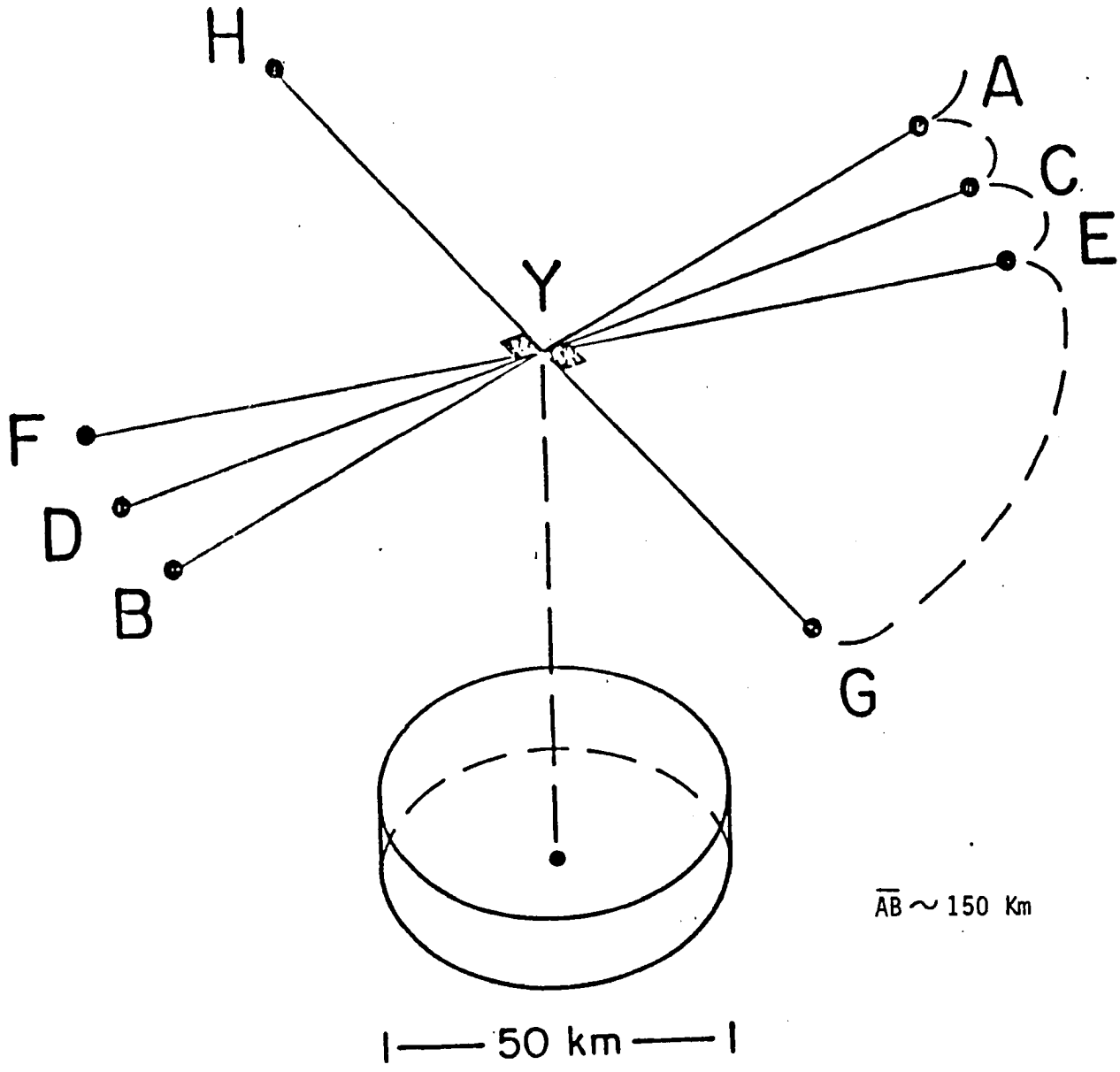

Figure A1. Radiation pattern R1 (Rosette).

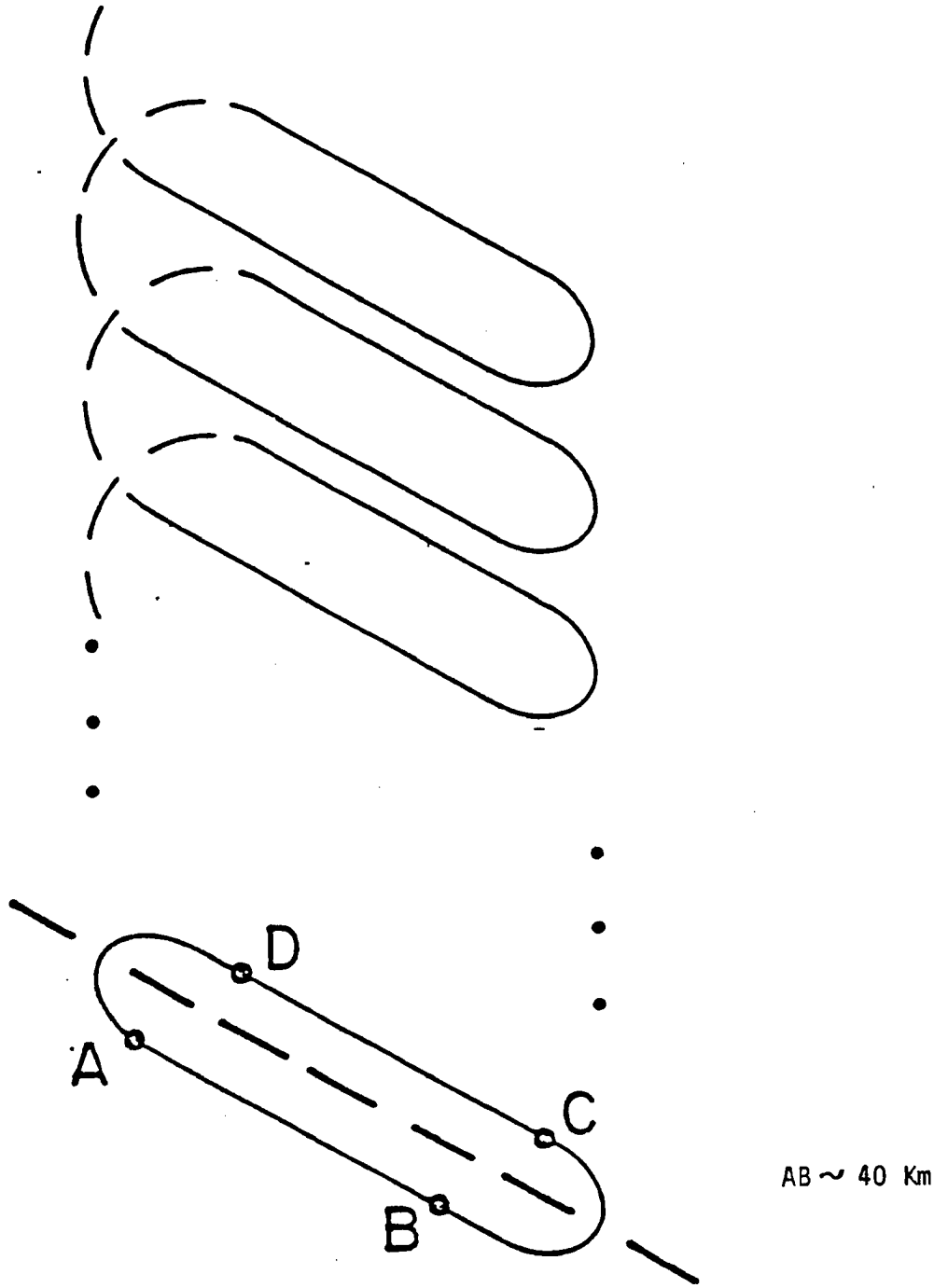

Figure A2. Radiation pattern R2 (Stepped race track).

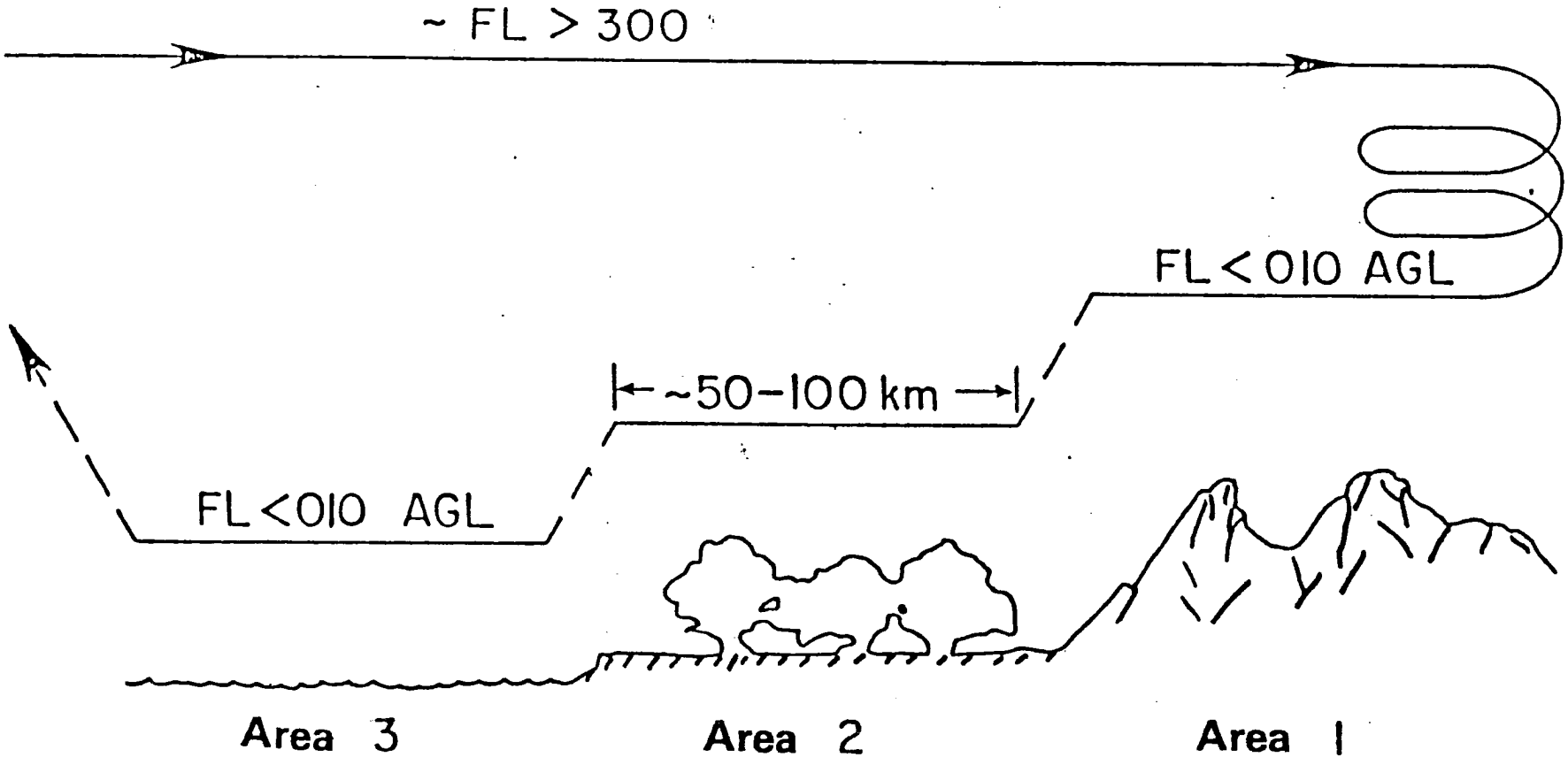

Figure A3. Radiation pattern R3 (albedo).

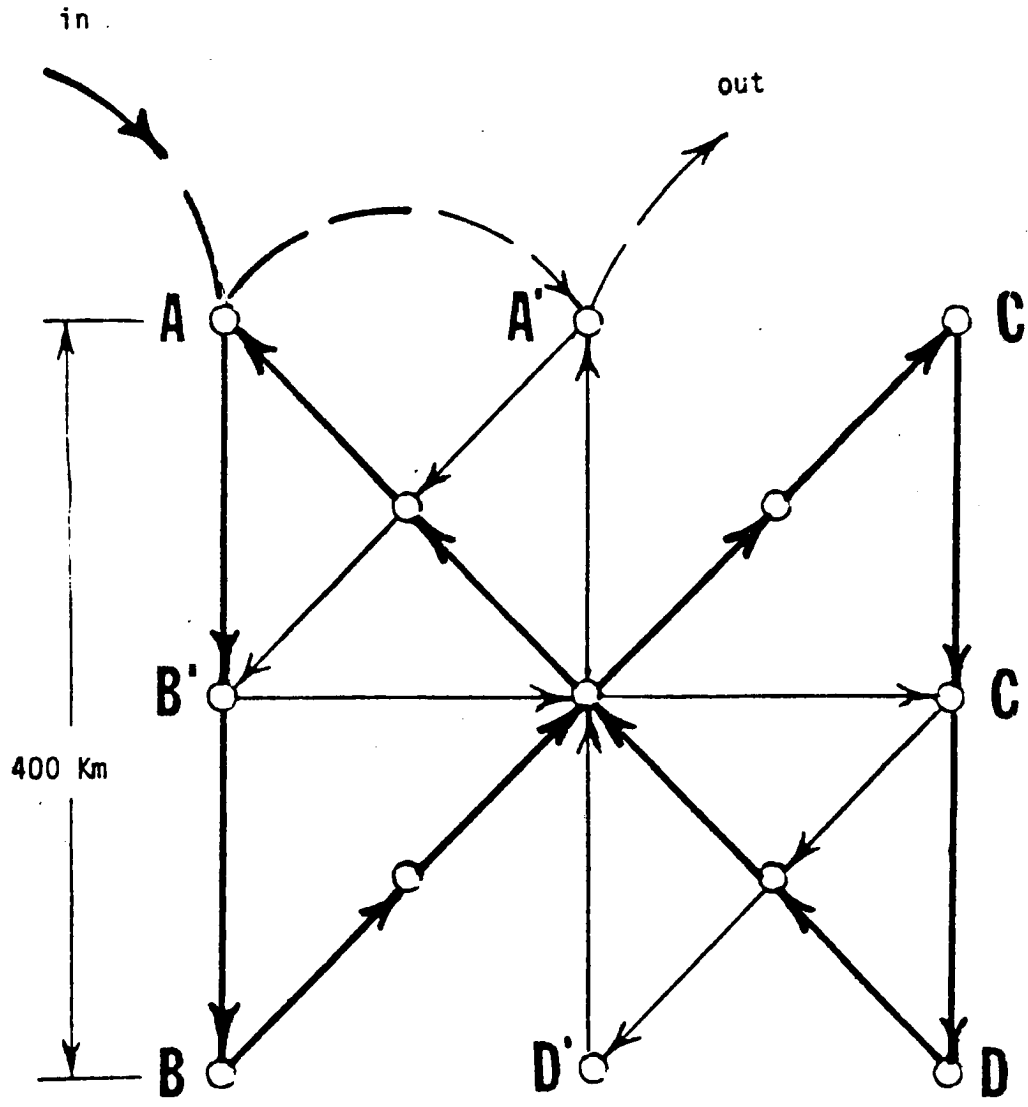

Figure A4. Radiation pattern R4 (budget).

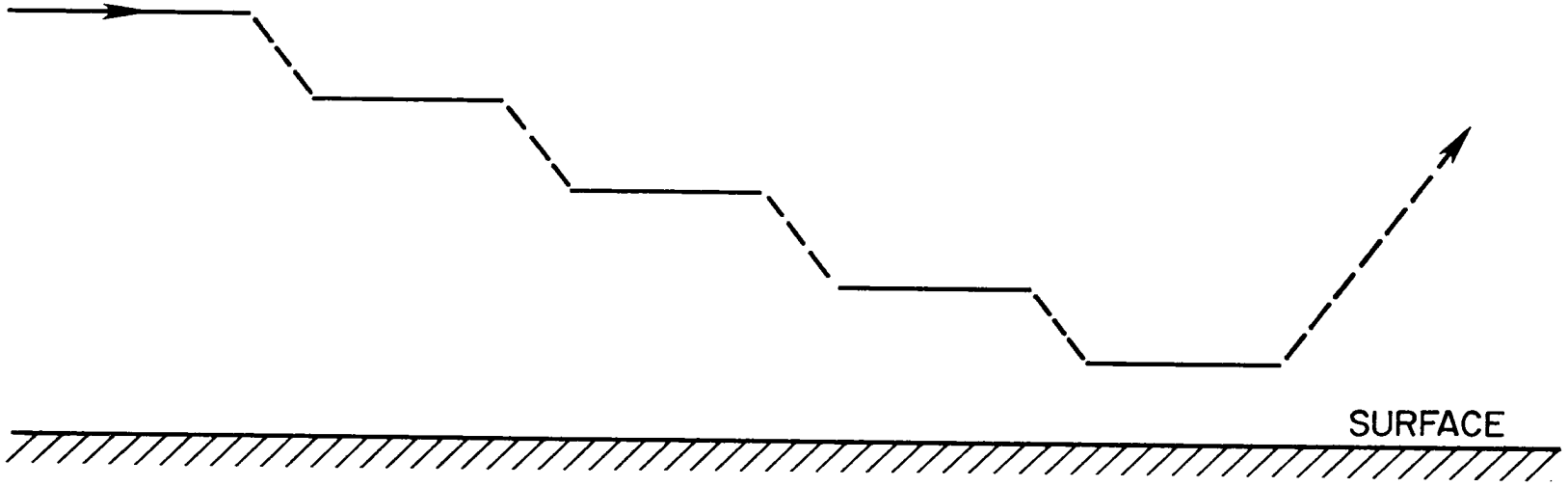

Figure A5. Stair-step vertical profiling.

APPENDIX B

COLORADO STATE UNIVERSITY SUMMER MONEX INSTRUMENTATION LOG

Tables B1 - B3 are the summer MONEX instrumentation logs for the pyranometers, pyrgeometers and PRT-6 respectively.

TABLE B1. PYRANOMETER LOG

DATE	POSITION ON AIRCRAFT	SERIAL NUMBER	REMARKS
April 30 (Flight 3)	Top front	12513	All pyranometers have WG7 domes (spectral band .3 - 2.8 μm). Acromag amplifiers on all pyranometers were set to following linear output: 0 mv input = .5V output 25 mv input = 10.5V output
	Top back	12515	
	Bottom left	12511	
	Bottom right	12512	500 Hz noise on the ADDAS. Lines were found on the second test flight (April 26, Day 116) that was not present during the first test flight (April 24). This noise was eliminated by removal of all the IC Buffer/Drivers and connecting the signals directly to ADDAS.
May 1 (Flight 4)			Strap on at following times (GMT): 12:33, 12:42, 13:17: 13:46, 14:34 Data were collected only over international waters.
May 3 (Flight 5)			Strap on Acromag inputs at following times (GMT): 9:25:31, 10:13, 10:51:20, 11:16, 12:42, 12:57.
May 5 (Flight 5)	Top front	12513	On reaching Dhahran the WG7 domes on pyranometers 12513 and 12512 were replaced with RG 695 domes (.695 - 2.8 μm).
	Bottom Right	12512	

TABLE B1. PYRANOMETER LOG

DATE	POSITION ON AIRCRAFT	SERIAL NUMBER	REMARKS
May 6 (Flight 6)			The strap on the Acromags was noted to be on at: 7:06, 7:38:44, 8:01, 8:24, 8:29, 8:49, 9:49, 10:09, 10:15, 11:05, 11:29, 11:34
∿ 9:49			ADDAS hung up. Back up at 9:53:10.
May 9 (Flight 7)	Top front	12513	Small scratch observed on pyranometer dome S/N 12513
			Strap was noted to be on at following times: 9:01, 10:02, 11:08, 11:21, 11:54, 12:11:36, 12:47, 13:26.
			ADDAS went down between 11:33:15 → 11:34:12
May 10 (Flight 8)	Bottom left Bottom right	12511 12512	Domes on the bottom pyranometers are slightly pitted.
			Strap was noted to be on at following times: 9:11, 9:13, 9:35, 10:11, 12:13, 12:48, 13:13, 13:29, 14:01.
May 12 (Flight 9)			Take-off time for this flight was 1:34:18 GMT, the sun had not yet risen thus output voltage of pyranometers was less than the electrical strap. Strap was noted to be on at: 1:50, 2:03, 2:09, 2:50, 4:08, 4:44.
May 14 (Flight 10)			During take-off pyranometer cables were not hooked up to ADDAS. Hooked up at 7:02 GMT
			Strap on at the following times: 7:37:27, 9:15.

TABLE B1. PYRANOMETER LOG

DATE	POSITION ON AIRCRAFT	SERIAL NUMBER	REMARKS
May 18 (Flight 11)			Strap observed to be on at the following times: 7:39, 9:09, (turned on for turns in racetrack pattern)
7:46:41			ADDAS down
7:47:46			ADDAS on line
May 29 (Flight 12)			Strap observed on at 7:04:20, 7:47, 8:51, 8:54.
May 30	Bottom Right	12514F3	The bottom pyranometer with the RG 695 dome was replaced with a different pyranometer (12514F3).
May 31 (Flight 13)			Strap on acromags noted to be on at 6:32, 6:57, 7:26, 8:02, 8:30.
June 3 (Flight 14)			Monitor Labs. appears noisy and .1 - .3V higher than EA. Strap on at approximately 5:18, 5:59:11.
June 5 (Flight 15)	Bottom pyranometers		Due to Indian security precautions, the downward looking instruments had to be "turned off" at specified times. For the bottom pyranometers, this was accomplished by disconnecting the input cables to the ADDAS. Today was the first day the Cipher tape recorder was up. All pyranometer output voltages were recorded. Sampling rate - 1 scan per second. Strap observed to be on at the following times: 5:42, 7:38, 7:57.

TABLE B1. PYRANOMETER LOG

DATE	POSITION ON AIRCRAFT	SERIAL NUMBER	REMARKS
June 5 (Flight 15)			
5:03:15			Downward instruments off (DIOFF)
5:11			Downward instruments on (DION)
5:24:50			DIOFF
5:51			DION
6:10			DIOFF
6:17:30			DION
6:54			DIOFF
7:05			DION (?)
7:19			DIOFF
8:13			DION
8:45			DIOFF
8:57			DION
9:22			DIOFF
June 7 (Flight 16)			Strap is on inputs from take-off until flight altitude is reached (∿ 4:22 GMT) Strap observed to be on at: 6:30, 7:31.
8:31	ADDAS		ADDAS had some problems, came back on line at 8:31.
June 8	12514F3 (Channel 0)		Top acromags recalibrated today.
	12511 (Channel 2)		
June 10	12513 (Channel 1)		Bottom acromags recalibrated using MV potentiometer at EA
	12515 (Channel 3)		

TABLE B1. PYRANOMETER LOG

DATE	POSITION ON AIRCRAFT	SERIAL NUMBER	REMARKS
June 11 (Flight 17)			
5:59	ML		Monitor Labs' tape recorder set at 1 sec. scans. Strap on at following times: 6:14, 8:30, 8:36, 9:03.
7:25	Bottom		Downward facing radiometers turned off.
7:31:48	Pyranometers		Downward facing radiometers turned on.
June 12 (Flight 18)			Strap noted to be on at the following times: 4:53.
5:02	ML		Monitor Labs' tape recorder on at 1 sec. scan intervals.
10:00	ML		Monitor Labs. shut down.
June 14 (Flight 19)	Bottom		Downward facing instrument must remain off, till way point 1.
5:43:40	Bottom		Downward radiometers on. Strap turned on during turns of Rosette.
June 15 (Flight 20)			
5:31			Downward looking radiometers turned on by turning off strap.
June 17 (Flight 21)	12514F3 (Channel 0)		Top acromags recalibrated today.
	12511 (Channel 2)		

TABLE B1. PYRANOMETER LOG

DATE	POSITION ON AIRCRAFT	SERIAL NUMBER	REMARKS
June 18 (Flight 22) 6:51			CV 990 had problems with two generators. As a result the EA, camera, and parts of ADDAS and other experiments were shut down.
June 22 (Flight 23)			Strap noted to be on at 6:42 and during turns of pattern.
June 23 (Flight 24)			Downward looking instruments turned on at 7:02.
7:57			Monitor Labs. tape on at 10 Hz scan interval. Strap on during turns in pattern.
June 26 (Flight 25)			Strap noted to be on at 8:42:42, 9:03
9:11:55 9:17 10:34			Cipher recording at 10 Hz ML display at time is bad. Cipher no longer recording.
June 27 (Flight 26)			Strap noted to be on at 7:38.
July 3 (Flight 28)	Top front Bottom left		WG7 domes replace RG 695 domes.

TABLE B1. PYRANOMETER LOG

DATE	POSITION ON AIRCRAFT	SERIAL NUMBER	REMARKS
June 11 (Flight 17)			
5:59	ML		Monitor Labs' tape recorder set at 1 sec. scans. Strap on at following times: 6:14, 8:30, 8:36, 9:03.
7:25	Bottom		Downward facing radiometers turned off.
7:31:48	Pyranometers		Downward facing radiometers turned on.
June 12 (Flight 18)			Strap noted to be on at the following times: 4:53.
5:02	ML		Monitor Labs' tape recorder on at 1 sec. scan intervals.
10:00	ML		Monitor Labs. shut down.
June 14 (Flight 19)	Bottom		Downward facing instrument must remain off, till way point 1.
5:43:40	Bottom		Downward radiometers on. Strap turned on during turns of Rosette.
June 15 (Flight 20)			
5:31			Downward looking radiometers turned on by turning off strap.
June 17 (Flight 21)	12514F3 (Channel 0)		Top acromags recalibrated today.
	12511 (Channel 2)		

TABLE B1. PYRANOMETER LOG

DATE	POSITION ON AIRCRAFT	SERIAL NUMBER	REMARKS
June 18 (Flight 22) 6:51			CV 990 had problems with two generators. As a result the EA, camera, and parts of ADDAS and other experiments were shut down.
June 22 (Flight 23)			Strap noted to be on at 6:42 and during turns of pattern.
June 23 (Flight 24) 7:57			Downward looking instruments turned on at 7:02. Monitor Labs. tape on at 10 Hz scan interval. Strap on during turns in pattern.
June 26 (Flight 25) 9:11:55 9:17 10:34			Strap noted to be on at 8:42:42, 9:03 Cipher recording at 10 Hz ML display at time is bad. Cipher no longer recording.
June 27 (Flight 26)			Strap noted to be on at 7:38.
July 3 (Flight 28)	Top front Bottom left		WG7 domes replace RG 695 domes.

TABLE B2. PYRGEOMETER LOG

DATE	POSITION ON AIRCRAFT	SERIAL NUMBER	REMARKS
April 30 (Flight 3)	Bottom pyrgeometer	12507	The settings on the bottom acromag are wrong.
	Top pyrgeometer	12508	Linearity of top acromag is set as follows: -3.0 mv input = .5 V output 1 mv input = 10.5 V output. 500 Hz noise on the ADDAS lines was eliminated by removal of all the IC Buffer/Drivers and connecting the signals directly to ADDAS Strap on acromag inputs was observed to be on at the following times (GMT): 18:20, 19:00, 19:15, 20:33, 21:37, 21:40, 22:04 Both pyrgeometers have silicon domes
May 1 (Flight 4)			Data collected over international waters only. Acromag strap was on at the following times: 12:33, 12:42, 13:17, 13:46, 14:34. Bottom acromag needs to be reset.
May 3 (Flight 5)			Bottom acromag reset to the following linear amplification: -3 mv input = .5 V output 1 mv input = 10.5 V output
May 6 (Flight 6)			ADDAS got hung up between 9:49 and 9:50, back on line at 9:53:10.

TABLE B2. PYRGEOMETER LOG

DATE	POSITION ON AIRCRAFT	SERIAL NUMBER	REMARKS
May 6 (Flight 6) (Continued)			Strap on acromag at following times: 7:06, 7:38, 8:01, 8:24, 8:29, 8:49, 9:49, 10:09, 10:15, 11:05, 11:29, 11:34.
May 9 (Flight 7)	Top and bottom		Black body calibration test prior to mission
11:33:15	ADDAS		ADDAS down, back up at 11:34:12. Strap was noted to be on at the following times: 9:01, 10:02, 11:08, 11:21, 11:54, 12:11, 12:47, 13:26.
May 10 (Flight 8)			Black body calibration test prior to mission. Strap was noted to be on at: 9:11, 9:13, 9:35, 10:11, 12:13, 12:48, 13:13, 13:29, 14:01.
May 12 (Flight 9)			Top and bottom black body calibration check. Strap on at: 1:50, 2:03, 2:09, 2:50, 4:08, 4:44.
May 14 (Flight 10)	Bottom		Some pitting noticed on bottom pyrgeometer dome. Black body test on top and bottom pyrgeometer prior to mission.
	Top and bottom		On take-off pyrgeometer cables were not plugged into ADDAS. Hooked up at 7:02.
			Strap on at the following times: 7:37:27, 9:15.

TABLE B2. PYRGEOMETER LOG

DATE	POSITION ON AIRCRAFT	SERIAL NUMBER	REMARKS
May 18 (Flight 11)			
7:46:41			ADDAS went down
7:47:46			ADDAS back up. Strap observed to be on at 7:39, 9:09, and for turns of racetrack.
May 21	Top pyrgeometer	12504F3	Both pyrgeometers replaced with different pyrgeometers. The present instruments have KRS 5 domes.
	Bottom pyrgeometer	12503F3	
May 29 (Flight 12)			Black body test prior to mission (May 28). Strap observed to be on at 7:04, 7:47, 8:51, 8:54.
May 31 (Flight 13)			Black body test prior to mission. Strap on acromags at 6:32, 6:57, 7:26, 8:02, 8:30.
June 3 (Flight 14)			Black body test on top and bottom pyrgeometers.
			Monitor Labs. appears noisy and .1 - .3 V higher than EA.
8:05			Double wing over Strap on at 5:18, 5:59.
June 5 (Flight 15)			Black body calibration test on top and bottom pyrgeometers.
	Bottom pyrgeometer		As a result of Indian security precautions, all downward looking instruments had to be turned off at specified locations.

TABLE B2. PYRGEOMETER LOG

DATE	POSITION ON AIRCRAFT	SERIAL NUMBER	REMARKS
June 5 (Flight 15) (Continued)			For the bottom pyrgeometer this was accomplished by disconnecting the input cables to the ADDAS.
			Today was the first day the Cipher tape recording system were up. Top and bottom pyrgeometer was recorded with a sampling rate of 1 scan per second.
			Strap observed on at 5:42, 7:38, 7:57.
5:03:15			Downward facing instruments off (DIOFF)
5:11			Downward facing instruments on (DION)
5:24:50			DIOFF
5:51			DION
6:10			DIOFF
6:17:30			DION
6:54			DIOFF
7:05			DION (?)
7:19			DIOFF
8:13			DION
8:45			DIOFF
8:57			DION
9:22			DIOFF
June 7 (Flight 16)			EA set up for a print out every 30 sec.
6:39	Bottom	12503F3	Lost the bottom pyrgeometer dome during a turn. Values for rest of flight are no good.
			Strap noted to be on at 6:30 and from take-off time to approximately 4:22.
June 8	Bottom pyrgeometer	12503F3	The bottom pyrgeometer dome that fell off in previous flight was replaced with a silicon dome. The same pyrgeometer casing was used.

TABLE B2. PYRGEOMETER LOG

DATE	POSITION ON AIRCRAFT	SERIAL NUMBER	REMARKS
June 8 (Continued)	Top pyrgeometer	12504	Top acromag calibrated.
June 10	Bottom pyrgeometer	12503F3	Bottom acromag recalibrated using millivolt potentiometer and EA.
June 11 (Flight 17)	Bottom pyrgeometer	12503F3	Black body calibration test on bottom pyrgeometer.
5:59	ML		1 sec. scans set on Monitor Labs.
7:25	Bottom pyrgeometer		Downward radiometers turned off for security reasons.
7:31			Downward facing radiometers turned on.
			Acromag strap on at following times: 6:14, 8:30, 8:36, 9:03.
June 12 (Flight 18)			
5:02	ML		Monitor Labs. tape recorder on at 1 sec. scan intervals.
10:00	ML		Monitor Labs. shut down.
			Strap noted to be on at 4:53.
June 14 (Flight 19)	Bottom		Black body test on top and bottom pyrgeometers. Downward instruments must remain off till way point 1.
5:43:40	Bottom		Downward facing radiometers on. Strap turned for turns in Rosette.
June 15 (Flight 20) 5:31			Downward facing radiometers turned on by turning off strap.

TABLE B2. PYRGEOMETER LOG

DATE	POSITION ON AIRCRAFT	SERIAL NUMBER	REMARKS
June 17 (Flight 21)			Strap noted to be on at 6:30.
June 18 (Flight 22) 6:51			CV 990 had problems with two generators. As a result the EA, camera and parts of ADDAS and other experiments were turned off.
June 22 (Flight 23)			Black body test on top and bottom pyrgeometers.
June 23 (Flight 24)	Bottom		Downward facing instruments turned on at 7:02.
7:57	ML		Monitor Labs. tape recorder on at 10 Hz scan interval. Strap on during turns in pattern.
June 26 (Flight 25)	Top	12504F3	Today was the first time we had a chance to check the instruments on top of the plane (since June 22). The top pyrgeometer has the appearance of being "sand-blasted" sometime since the beginning of Flight 23, no time to replace dome.
9:11:55	ML		Cipher tape recorder on, recording at 10 Hz scan interval.
9:17			ML display of time is bad.
10:34	ML		Cipher no longer recording.
June 27 (Flight 26)			Strap rate to be on at 7:38.

TABLE B3. PRT-6 LOG

DATE AND TIME	REMARKS
April 30 Flight 3	PRT-6 will not be turned on until Dhahran
May 6 Flight 6	Settings for PRT-6 are as follows: Attenuation = 6 ETO = 5.2
	PRT-6 shutter is closed for this flight.
8:57	PRT-6 shutter opened.
9:49	ADDAS down. Back up at 9:53:10.
12:13	PRT-6 shutter closed.
May 9 Flight 7	PRT-6 shutter opened at 10:29.
11:33:15	ADDAS down. Back up at 11:34:12.
May 10 Flight 8	PRT-6 shutter was opened after take-off.
9:25:10	PRT-6 shut off to reduce wear on chopper motor.
13:43	PRT-6 turned on for descent.
May 14 Flight 10	During this flight it was discovered that the PRT-6 output voltages were not reaching ADDAS. This error was corrected at 8:15.
May 18 Flight 11	
8:38:11	PRT-6 shut off at 33 k feet.
9:15	PRT-6 turned on.
11:22	PRT-6 shut off.
May 29 Flight 12	
5:35	PRT-6 on, shutter will be opened when cavity is warmed up.
9:14	PRT-6 shut off.
10:48	PRT-6 turned on.
May 31 Flight 13	
5:39:38	PRT-6 shutter opened.
6:44	PRT-6 shut off.
9:00:25	PRT-6 turned on.
10:14:30	PRT-6 shut off.
June 5 Flight 15	PRT-6 turned on at 6:22:14.

TABLE B3. PRT-6 LOG

DATE AND TIME	REMARKS
June 7 Flight 16	PRT-6 turned on at 3,000', shutter opened at 8,000'.
5:27	PRT-6 off.
6:30	PRT-6 turned on approximately 10-15 min. ago.
7:38	PRT-6 shut off.
8:31	ADDAS had some problems around this time.
June 11 Flight 17	
5:43	PRT-6 shutter opened.
5:59	1 sec. scans set on Monitor Labs.
June 12 Flight 18	ML recorded from 5:02 to 10:00 at 1 sec. scan intervals.
June 22 Flight 23	
7:09	ML recorder on at 1 sec. scan interval.
June 26 Flight 25	PRT-6 shutter opened at 7:20.
June 27 Flight 26	Shutter opened at 6:05:04.

APPENDIX C

TAPE FORMAT OF COLORADO STATE UNIVERSITY REDUCED RADIOMETRIC DATA

The reduced tapes consist of the 1 second values of a variety of parameters. These parameters are listed in Table C1. The parameters should be "buffered" in the given order with odd parity. Each record represents a 1 second time interval. The NCAR and Colorado State University tape numbers corresponding to a given flight are listed in Table C2.

VARIABLE	UNITS AND COMMENTS
Latitude	In degrees
Longitude	In degrees
Julian Day	Integer format
Hour (GMT)	Integer format
Minute (GMT)	Integer format
Second (GMT)	Read format
Pressure altitude	In feet corresponding to U.S. Standard Atmosphere, 1962
Radar altitude	In feet above ground
Static air temperature #1	In degrees Kelvin directly from CADC*
Static air temperature #2	In degrees Kelvin computed from the mach number and total air temperature (SAT #2 has less noise and more accuracy than SAT #1)
Specific humidity	In g kg^{-1}
Dew/frost point	In degrees celcius. There are two caution flags attached to this parameter. If the hygrometer is at maximum heating -2000 is added to the DFP, if the hygrometer is at maximum cooling, -1000 is added to the determined DFP
Pressure	In mb, computed from pressure altitude and U.S. Standard Atmosphere, 1962
Incoming .7 - 2.8 μm radiation	In watts m^{-2}, determined using constant correction for optical zero offset
Outgoing .7 - 2.8 μm radiation	In watts m^{-2}, determined using constant correction for optical zero offset
Incoming .3 - 2.8 μm radiation	In watts m^{-2}, determined using constant correction for optical zero offset
Outgoing .3 - 2.8 μm radiation	In watts m^{-2}, determined using constant correction for optical zero offset
Incoming .7 - 2.8 μm radiation	In Wm^{-2}, determined using pyrgeometer $T_D - T_S$ correction for optical zero offset

Table C1. (Page 1.)

VARIABLE	UNITS AND COMMENTS
Outgoing .7 - 2.8 μm radiation	In Wm^{-2}, determined using pyrgeometer $T_D - T_S$ correction for optical zero offset
Incoming .3 - 3 μm radiation	In Wm^{-2}, determined using pyrgeometer $T_D - T_S$ correction for optical zero offset
Outgoing .3 - 3 μm radiation	In Wm^{-2}, determined using pyrgeometer $T_D - T_S$ correction for optical zero offset
Incoming 4 - 50 μm radiation	In Wm^{-2} determined by using laboratory derived values of K_1 and K_2
Outgoing 4 - 50 μm radiation	" " " " "
Incoming 4 - 50 μm radiation	In Wm^{-2} determined by using the field derived values of K_1 and K_2
Outgoing 4 - 50 μm radiation	" " " " "
Surface temperature	In degrees centigrade determined from PRT-5 radiometer
Bugeye	In volts, this variable is dimensioned as a 26 element array
Heading	Aircraft true geodetic heading in degrees from INS
Pitch angle	In degrees from INS
Roll angle	In degrees from INS
Track angle	In degrees from INS
True airspeed	In knots from CADC*
PRT-6	In volts, this variable is dimensioned as a 24 element array. The first ten array elements contain the PRT-6 outputs resulting from the 10 Hz sampling rate. The second ten elements are the corresponding heater supply voltages. Element 21 is a dummy variable while element 22 is a voltage representative of the shutter temperature. Elements 23 and 24 are reference voltages of approximately +10 and -10 V.

*CADC = Central Air Data Computer

Table C1. Sequential list of variables stored on magnetic tape.

FLIGHT NUMBER	C.S.U. TAPE NUMBER	NCAR TAPE NUMBER
6	A1348	V36097
7	A1450	V36098
8	A1464	V36099
9	A1481	V36109
10	A1490	V36112
11	A1447	V0668
12	A1497	V36114
13	A1512	V36115
14	A1516	V36116
15	A1466	V36100
16	A1467	V36101
17	A1468	V36102
18	A1469	V36103
19	A1472	V36104
20	A1475	V36105
21	A1478	V36106
22	A1479	V36107
23	A1480	V36108
24	A1483	V36110
25	A1489	V36111
26	A1492	V36113

Table C2. Reference tape numbers corresponding to the reduced data of a given flight.

BIBLIOGRAPHIC DATA SHEET	1. Report No. CSU-ATS-325	2.	3. Recipient's Accession No.
4. Title and Subtitle Colorado State University Radiation Instrumentation and Data Reduction Procedures for the Convair 990 during Summer MONEX.			5. Report Date April, 1980 6.
7. Author(s) Steven A. Ackerman and Stephen K. Cox			8. Performing Organization Rept. No. CSU-ATS-325
9. Performing Organization Name and Address Department of Atmospheric Science Colorado State University Fort Collins, CO. 80523			10. Project/Task/Work Unit No. 11. Contract/Grant No. ATM-78-12631
12. Sponsoring Organization Name and Address National Science Foundation, NOAA			13. Type of Report & Period Covered 14.

15. Supplementary Notes

16. Abstracts

The basic system design and the radiative instrumentation maintained by Colorado State University on board the Convair 990 jet aircraft during the Summer Monsoon Experiment (MONEX) are described. Calibration procedures are discussed in detail and the derived constants used to convert instrument output to engineering units are given. Specific problems encountered during data reduction and the methods used to overcome them are also discussed. This report should assist meticulous users of the radiation data in obtaining a high quality data set.

17. Key Words and Document Analysis. 17a. Descriptors

MONEX radiative instrumentation
MONEX aircraft radiation data reduction

17b. Identifiers/Open-Ended Terms

17c. COSATI Field/Group

18. Availability Statement	19. Security Class (This Report) UNCLASSIFIED	21. No. of Pages 72
	20. Security Class (This Page) UNCLASSIFIED	22. Price

FORM NTIS-35 (Rev. 3-72)